IONTOPHORETIC DELIVERY OF CYTOTOXIC AGENTS FOR THE TREATMENT OF SOLID TUMORS

James Byrne

A dissertation submitted to the faculty of the University of North Carolina at Chapel Hill in partial fulfillment of the requirements for the degree of Doctor of Philosophy in the Division of Molecular Pharmaceutics in the UNC Eshelman School of Pharmacy

Chapel Hill
2014

Approved by

Joseph M. DeSimone

Jen Jen Yeh

Joel Tepper

Leaf Huang

Rudy Juliano

ABSTRACT

James Byrne: Iontophoretic delivery of cytotoxic agents for the treatment of solid tumors
(under the direction of Joseph M. DeSimone)

Parenteral and oral routes have been the traditional methods of administering cytotoxic agents to cancer patients. Unfortunately, the maximum potential effect of these cytotoxic agents has been limited due to systemic toxicity and poor tumor perfusion. In an attempt to improve the efficacy of cytotoxic agents while mitigating their side effects, we have developed modalities for the localized iontophoretic delivery of cytotoxic agents. These pressurized, reservoir-based iontophoretic devices were designed to be implanted proximal to the tumor with external control of power and drug flow. Three distinct orthotopic mouse models of cancer and a canine model were evaluated for device efficacy and toxicity. In the mouse models, device delivery of cytotoxic agents resulted in enhanced drug accumulation in the tumor and tumor shrinkage. In dogs, device delivery resulted in large local drug concentrations and low systemic drug exposure. These devices have potential paradigm shifting implications for the treatment of pancreatic, breast, and other solid tumors.

ACKNOWLEDGEMENTS

I would like to acknowledge all of the individuals who contributed to my work. Raheel Jajja was a fantastic colleague whose persistence and thoughtfulness enabled our success with both gemcitabine and FOLFIRINOX. Adrian O'Neill and Lissett Bickford assisted in the development of the implantable and transdermal devices, and their contributions were critical to the success of the project. Charlene Ross, the animal studies core, and the patient-derived xenograft core helped conduct many *in vivo* studies.

I have been fortunate to have many great mentors. My advisor, Joseph DeSimone, has provided me guidance in becoming an academician, entrepreneur, and family man, and he continually challenged me professionally and gave me phenomenal opportunities to grow as a scientist and engineer. Jen Jen has been a fantastic mentor, who constantly pushed me to ask the right questions, use evidence rather than theory to guide experimentation, and focus upon both the small details in my experimentation and presentation of my work. Joel Tepper provided significant guidance in my dissertation work and has been great support in my career aspirations. Leaf Huang taught me a great deal from my laboratory rotation, and he and Rudy Juliano have continued to provide significant mentorship as part of my dissertation committee. Mary Napier and Chris Luft have always been extremely supportive in the day-to-day operations of the DeSimone lab.

Finally, I would like to acknowledge my parents, Mike and Elaine, and wonderful fiancée, Maggie McGinn, for their continued support of my pursuits in science and medicine.

TABLE OF CONTENTS

LIST OF EQUATIONS

LIST OF FIGURES

LIST OF ABBREVIATIONS

Ag/AgCl – silver/silver chloride

Pt - platinum

F – Faraday's constant

A – cross-sectional area

I - current

t_x – transport number of drug X

I_D – current density

z_x – charge of drug X

u_x – mobility of drug X

c_x – concentration of drug X

L_{ii} – Onsager coefficient

pI – isoelectric point

µL – microliter

cm - centimeter

h - hour

µg – microgram

mL - milliliter

MMC – mitomycin C

EMDA – electromotive drug administration

PD – passive diffusion

BCG – Bacillus Calmette-Guerin

C_{max} – maximum concentration

IV – intravenous

mA – milliamperes

g – gram

µg – microgram

VT – ventricular tachycardia

TAT-59 – miproxifen phosphate

DP-TAT-59 – dephosphorylated metabolite of miproxifen phosphate

mm – millimeter

wt% - weight percentage

min – minute

PEDOT – poly(3,4 – ethylenedioxythiophene)

PDX – patient-derived xenograft

UV – ultraviolet

HPLC – high performance liquid chromatography

PK – pharmacokinetics

3D – three-dimensional

kg – kilogram

AUC – area under the curve

NaCl – sodium chloride

BUN – blood urea nitrogen

FOLFIRINOX – Folinic acid, 5-fluorouracil, irinotecan, oxaliplatin

THU – tetrahydrouridine

IRB – Institutional review board

IACUC – Institutional animal care and use committee

M – molar

v/w – volume/weight

rpm – rotations per minute

2’dC – 2’deoxycytidine

mM – millimolar

ng – nanogram

Gy – gray

ICP-MS – inductively coupled mass spectrometry

ANOVA – analysis of variance

SEM – standard error measurement

NS – not significant

CHAPTER 1: INTRODUCTION

1.1 Overview of Iontophoresis

As an electric field is generated across a conducting medium, a force is exerted on charged particles that exist within that medium. If the particles are able to move, the force results in an electric current. In metals, the force is exerted on conduction band electrons and the result is an electronic current. In ionic solutions, such as saline, the force is exerted on ions and the result is ionic current.

Iontophoresis is a hybrid of these two currents established by an electric field. A power source is used to establish the electric field through an anode (positive electrode) and cathode (negative electrode) (Figure 1.1). The anode is at the highest potential and each successive point in this circuit is at a lower potential, and the cathode is the lowest potential point. The resulting electric fields cause electrons to migrate in the direction of the battery anode in the electronic portions of the circuit and causes ions to flow in the ionic solution portion of the circuit - positive ions moving toward the cathode and negative ions toward the anode. The ionic solution portion of the circuit is comprised of the anode reservoir, hydrated tissue between the anode and cathode reservoirs, and the cathode reservoir. The current flowing in the ionic parts of the circuit has two components: cations moving toward the cathode and anions moving toward the anode. If there are more than one species of cation or anion each species will contribute to the overall current depending on its concentration and mobility. At any surface drawn perpendicular to the direction of current flow, the total

number of ions passing through that surface per unit time must equal the current being delivered by the battery.

If the solution of ions in the anode or cathode reservoir contains a therapeutic agent, then it will migrate in the direction of the opposite electrode and hence into the tissue. Thus, the applied electric field accomplishes drug delivery. Because of the ease with which the magnitude of the electric field can be changed, there are many advantages to this form of drug delivery [1].

1.2 History of Iontophoresis

The first proposed use of an electric field for drug delivery dates back to the mid-18th century from Johann Gottlob Krueger [2]. Krueger stated that electricity should be "useful in medicine, as it was obviously not useful for theology or jurisprudence." The first experimental evidence of the use of electric fields for drug delivery purposes was obtained in 1747 by Giovanni Francesco Pivati [3]. Throughout the late nineteenth century, significant progress was made in the transdermal iontophoretic delivery of a variety of drugs, including atropine, quinine, lithium salts, and cocaine. In the 1930s, Elkin Percy Cumberbatch dictated the limitations of this method, which was principally the shallow depth ions are able to reach in tissues [4]. Cumberbatch and others proposed the application of ionic medication to organs other than the skin, including the urethra, middle ear, and cervix (Figure 1.2) [4-6]. Although these iontophoretic devices were generated for non-transdermal drug delivery, the predominant focus was on the transdermal application of iontophoresis.

1.3 Iontophoretic Electrochemistry

There exist many different types of electrodes used in iontophoretic drug delivery. The two major types are classified according to their electrochemistry as reversible electrodes (silver/silver chloride (Ag/AgCl)) and inert electrodes (platinum) [7-9]. For Ag/AgCl electrodes, the electrochemistry occurring at the Ag anode requires the presence of Cl^- ions in the anodal compartment (Figure 1.3). Without the presence of the Cl^- ions, Ag^+ ions are transported with the drug. The requirement of the Cl^- ions can reduce the efficiency of drug delivery since highly mobile Na^+ ions can compete very effectively with the drug to carry current; however, there are many water soluble drugs that are formulated as hydrochloride salts, which alleviates the need for the addition of NaCl. As the Cl^- ions arrive at the electrode–solution interface, they react with the metallic silver to form silver chloride, which on account of its low solubility product, is deposited at the electrode surface, simultaneously releasing an electron. In order to maintain electroneutrality in the anodal compartment, either a cation must move out of the compartment and into the tissue or an anion must leave the tissue and move into the anodal chamber. In the cathodal compartment, the AgCl is reduced by the arrival of electrons from the power supply and yields metallic silver together with a Cl^- ion, which passes into the solution, which must be compensated for by the arrival of a cation from within the tissue into the cathodal chamber or by the loss of an anion. One major advantage of Ag/AgCl electrodes is that the electrochemistry occurs at voltages lower than those necessary for the electrolysis of water. This is desirable since protons created at the anode of non-Ag/AgCl materials compete to carry charge and because of their small size and high mobility, they may significantly reduce drug delivery efficiency;

moreover, the low pH produced in the anodal compartment can lead to acid-induced burns, and it may have an adverse effect on drug stability.

For Pt electrodes, the electrochemistry occurring at the Pt interface induces electrolysis during the release of electrons (Figure 1.3). This effectively reduces the pH around the electrode, which could severely impact the stability of the drug, drug delivery efficiency, and the integrity of the surrounding tissue depending upon the design of the electrode [10]. The advantage of Pt electrodes is that the electrode is relatively inert and does not breakdown in the same manner as Ag/AgCl electrodes.

1.4 Iontophoretic Transport Mechanisms

The observed iontophoretic flux of a charged species, X, at steady-state can be considered as the sum of two separate transport mechanisms – electromigration and electroosmosis, assuming that the passive permeability is negligible (Equation 1). Electromigration refers to the ordered movement of ions in the presence of the applied electric field. The electromigratory flux of an ion, X, is related to the component current flow i_x due to its transport by Faraday's constant, F, where A represents the cross-sectional area for transport across tissue and z_x is the charge (Equation 2). The ionic current flow due to the movement of X can be related to the applied current, I, by a proportionality constant, t_x, the transport number of X ($0 < t_x < 1$), which describes the fraction of the total current transferred by X (Equation 3).

The transport number of X depends on the physicochemical properties of X and how these changes with the corresponding properties of the other charge carriers present in the system. Specifically, where I_D is the applied current density (= I/A) and z_x, u_x, and c_x refer to

the charge, mobility and concentration of the drug in the membrane, respectively (Equation 4); the denominator is the sum of the products of these parameters for each ion in the system contributing to charge transfer across the membrane. This form of the transport equation explains why the presence of competing ions can reduce the drug flux and delivery efficiency. Furthermore, the extent of competition and attenuation of drug transport will depend on the products of the respective electrical mobilities and concentrations in the membrane. Increasing the concentration of a less mobile drug species can improve delivery efficiency in the presence of a small highly mobile competing ion.

The electroosmotic component is based upon non-equilibrium thermodynamics. Pikal has analyzed the phenomenon in considerable depth and elegantly described how the application of pressure and a potential difference across a membrane can be used to generate current and volume flows, respectively [11-14]. The two flow phenomena can be expressed as found in Equation 5.

The flows are related to their causal or conjugate forces, by the respective Onsager coefficients, L_{ii}; L_{11} gives the volume flow in response to the application of a pressure gradient and L_{22} is the proportionality constant relating the potential difference to the current. The cross coefficients L_{ij} describe interaction terms. Thus, L_{12} defines how application of a potential difference across a membrane will create a volume flow. In an iontophoretic experiment when an electric field is applied across the tissue, $\Delta Pressure = 0$, electroosmotic flow is equivalent to volume flow divided by current flow (Equation 6).

Electroosmosis can be explained as the volume flow induced by the current flow. At a molecular level, electroosmosis can be viewed as resulting from the fact that the tissue has an isoelectric point (pI) ~ 4–4.5 [15], above which the carboxylate groups present in the

membrane become ionized. Application of an electric field across a charged membrane favors the movement of counter-ions that try to neutralize the membrane charge and gives rise to its cation permselectivity. Electroosmosis can be defined either as a flow process that is volume flow per unit area per unit time or as a solvent velocity, v, and it is equivalent to a permeability coefficient with corresponding units. The existence of this solvent flow in the anode-to-cathode direction means that (i) neutral molecules can be delivered by anodal iontophoresis and (ii) cations will benefit from a second driving force in addition to electromigration. The total flux of X, a cationic drug, is shown in Equation 7.

From these equations, it would appear that iontophoretic flux should increase with drug concentration and with applied current; the patch area can also be enlarged to further increase the amount of drug delivered. The relative importance of electromigration and electroosmosis to the total flux of a molecule depends on its physicochemical properties. Electrical mobility will decrease with molecular weight and the electroosmotic contribution is increasingly important for larger molecules (Figure 1.4) [16].

1.5 Modern Iontophoretic Technologies

Many researchers have utilized iontophoretic drug delivery systems to increase locoregional drug concentrations while abating toxic systemic side effects associated with current intravenous, oral, and passive administrations. Numerous device studies have been conducted for the local and systemic delivery of drugs by iontophoresis through skin, non-muscle invasive bladder tumors, ocular tissue, restenotic vessels, and myocardial tissue. A number of the delivery systems have gained regulatory approval from the United States Food and Drug Administration and the European Medicines Agency [17].

1.5.1 Transdermal

Transdermal drug delivery has been the most well-studied application within the field of iontophoresis, and there have been a plethora of transdermal iontophoretic devices for the local and systemic delivery of drugs. Prime examples include devices that have been developed for delivering lidocaine to promote local anesthesia (LidoSite®) seen in Figure 1.5, administering fentanyl to treat systemic pain (Ionsys™), and monitoring glucose levels in diabetics (GlucoWatch Biographer™) [17]. Overall, there are hundreds of examples of transdermal iontophoretic drug delivery studies in the literature and many associated patents filed for these iontophoretic devices [18].

1.5.2 Transscleral

Ocular iontophoresis addresses the issues of low bioavailability of drugs after topical administration and the complexities of intraocular injections [19]. Due to the ease and safe delivery of drugs by ocular iontophoresis, clinical use of this treatment has become more extensive, resulting in technologies that improve drug delivery to the eye.

Numerous studies have been conducted that have shown that the penetration and retention of drugs in the eye through iontophoresis is greater than that of standard topical and subconjunctival administrations [19]. Grossman *et al.* conducted an analysis of the delivery of gentamicin to the anterior cornea, aqueous humor and vitreous in rabbits, comparing a subconjunctival injection to transscleral and transcorneal iontophoresis [20]. After 2 hours, the gentamicin delivered by transcorneal iontophoresis peaked in the cornea at 376.1 μg/ml and reached an average level of only 28.1 μg/ml by subconjunctival administration. The C_{max}

of transcorneal iontophoretic penetration in the aqueous humor was 54.8 μg/ml, which was 4 times higher than the peak drug penetration from subconjunctival injection. The C_{max} of transscleral iontophoretic gemtamicin levels in the vitreous was 20 times higher than drug levels produced by subconjunctival drug administration. Ocular iontophoretic studies have evaluated the delivery of antibiotics, antiviral drugs, antifungal drugs, steroids, and oligonucleotides. This emerging ophthalmic treatment provides an innocuous way to deliver drugs, eliminating the poor drug delivery to posterior portions of the eye seen with topical administrations and the complexities and pain associated with subconjunctival injections.

The novel field of nanoparticle delivery is offering another method of ophthalmic drug delivery when used in conjunction with ocular iontophoresis. Studies by Eljarrat-Binstock *et al*. examined the transport of positively and negatively charged particle delivery by electrophoresis compared to nanoparticle delivery by passive diffusion [21]. Hydrogel reservoirs filled particle suspensiosn were placed directly on the eye; three groups received positively charged particles through cathodal electrophoresis, one group acquired negatively charged particles through anodal electrophoresis, and two groups received either positively or negatively charged particles through passive diffusion. Through studies in rabbits, large particles concentrations were observed in the eye due to electrophoretic transport, though positively charged particles exhibited higher penetration into ocular tissues than did negatively charged particles. Moreover, nanoparticles could be of particular benefit through controlled drug release into tissues, possibly providing an answer for the delivery of non-ionized drugs or drugs with high molecular weights and poor ocular tissue penetration [21].

Ocular iontophoretic devices are now being manufactured by companies including Eyegate®, Visulex™ and OcuPhor™. The devices typically consist of eye cups and drug-

loaded hydrogels to deliver drugs by iontophoresis. Eye cups are composed of a port that delivers the drug, and a metal electrode that controls the current supply and aspirates bubbles to keep the eye cup in place (Figure 1.5B). There is a reservoir located in the cup that continuously imbues the drug solution into the eye, allowing for a controlled and localized delivery [19]. Hydrogel applicators have been fabricated by Visulex™ and OcuPhor™ to optimize ocular drug delivery. The OcuPhor™ hydrogel consists of a drug saturated gel that is placed into a reservoir and a metal electrode, which allows for a mild current to transport drugs through the eye. Visulex™ has expanded upon this ocular iontophoretic hydrogel model by creating a selective membrane that increases the mobility of drug molecules across ophthalmic tissues by limiting non-drug current carrying ion transport [19]. Eyegate® has created transscleral iontophoretic delivery systems that have enabled the application of drugs to the anterior and posterior chambers of the eye [22]. New manufactured ocular iontophoretic devices are enhancing the delivery of drugs, allowing for a safer and more effective method of treatment for ophthalmic diseases.

1.5.3 Intravesical

Intravesical delivery of mitomycin-C (MMC) to non-muscle invasive bladder cancer has been the source of a myriad of studies aimed to enhance the efficacy of local drug delivery to tumors. Electromotive drug delivery (EMDA), also known as iontophoresis, offers a way to increase localized drug delivery to tumors, eliminate systemic side effects and lengthen remission rates and disease-free intervals [23].

Electromotive drug administration has led to increased efficacy of MMC delivery compared to the standard therapy of passive diffusion (PD) to treat bladder malignancies. Di

Stasi *et al*. examined the penetration of MMC in the urothelium *ex vivo*, comparing the efficacy of PD and EMDA delivery [24-25]. The electromotive administration resulted in increased local MMC delivery and penetration compared to PD; a four-fold to seven-fold increase in the rates of EMDA delivery of MMC was observed [24]. In a patient study by Rieldl *et al.*, transurethral resection was followed by intravesical delivery of MMC by EMDA [26]. After 14.1 months, 9 of the 16 patients were free of recurrent bladder cancer, and systemic side effects that are associated with standard MMC drug administration did not occur. Clinical studies comparing PD and EMDA of MMC are few, but the studies that have been conducted have resulted in better efficacy for patient's treated by EMDA compared to PD.

Data has suggested that the transport of MMC by EMDA is an alternative to or at least equivalent in effectiveness to the standard Bacillus Calmette-Guerin (BCG) treatment of care, which stimulates an immune response in the bladder to destroy malignant cells [27]. Di Stasi *et al.* conducted a randomized study to evaluate the efficacy of EMDA/MMC, BCG, and PD [28]. One hundred and eight patients received a 6 week treatment; three groups received either one instillation of 40 milligrams (mg) MMC by PD, a single 30 minute EDMA delivery of 40 mg of MMC under a current of 20 mA, or 2 BCG instillations of 81 mg. The efficacy of EDMA/MMC and BCG treatments was greater than PD, but there was little difference between EMDA and BCG, which suggests that EDMA could possibly be used as an alternative to BCG in treating bladder cancer [29]. The plasma concentrations of MMC by EMDA reached a C_{max} that was 5.5 times greater than PD of MMC, concluding that the efficacy of transmembranous drug transport is enhanced by localized electromotive delivery.

When BCG and EDMA/MMC are used in conjunction, there is an enhancement in effect compared to only BCG or EMDA/MMC treatments [27]. In a study by Di Stasi et al., patients were treated with BCG and EMDA/MMC sequentially, testing the hypothesis that the convergence of two therapies could act synergistically, improving the overall therapeutic efficacy. The studies proved that patients who received BCG and EMDA/MMC sequentially had a longer disease-free interval than patients who only received BCG. All 78 of stage T1 patients who received both therapies did not see a recurrence of disease after 3 months compared to the recurrence of bladder cancer in 3 of the 75 patients who received only BCG. After 88 months, 106 of the patients were disease-free: 41.9% received only BCG and 57.9% received sequential deliveries of BCG and EDMA/MMC. During a follow up, 23 deaths due to bladder cancer occurred: 17 in the BCG group and 6 in the BCG and EDMA/MMC group. Side effects were localized in the bladder and the toxicity of both treatments was very similar. The results of the Di Stasi studies led to the conclusion that sequential delivery of BCG and EDMA/MMC can increase survival and disease-free intervals [27].

1.5.4 Transmyocardial

The adverse systemic side effects associated with current drug administration to treat arrhythmias have prompted the development of novel iontophoretic devices to deliver drugs locally to cardiac tissues [30]. Transmyocardial iontophoretic drug delivery offers a way to increase drug penetration, effectively targeting the affected tissues.

Studies have evaluated the efficacy of iontophoretic drug delivery to the myocardium compared to that of standard-of-care approaches. In a study by Avitall B *et al*., procainamide was delivered via iontophoresis to canine models through an implantable defibrillator patch

electrode (9 mA), passive diffusion (PD), and intravenous (IV) administration for a ten minute delivery period [30]. Procainamide concentrations in the epicardial layer were 840 μg/g, 93 μg/g and 15 μg/g 3 hours after iontophoretic, PD and IV administrations, respectively. IV doses used were 15 mg/kg followed by 0.6 mg/kg/min for 3 hours, which was similar to human dosing. Iontophoretic drug delivery resulted in lower levels of procainamide in the blood (2 ± 3 μg/g) compared to intravenous levels (11 ± 7 μg/g), though passive diffusion resulted in the lowest systemic drug levels (1 ± 1 μg/g). In all canine models that received iontophoretic procainamide delivery, ventricular tachycardia (VT) was rapidly suppressed and sustained for 60 minutes, and in 7 of 10 dogs, VT was suppressed for 3 hours. The effective refractory period and the diastolic threshold did not significantly increase due to iontophoretic procainamide delivery. In another canine study by Labhasetwar *et al.*, a heterogenous cation-exchange membrane was used in the iontophoretic transport of *dl*-sotalol hydrochloride from an epicardial reservoir sutured onto the myocardium [31]. The study determined that the release rate of the drug from the device was linearly correlated with the current applied, and peak coronary sotalol levels positively correlated with the applied current.

Though local iontophoretic drug transport directly to the myocardium improves delivery efficacy due to the low resistance of cardiac tissues, there is still potential for optimizing devices and transport. Parameters, including drug concentration, drug type, duration of drug transport, and electrode size and configuration, still needs to be evaluated to determine optimal delivery [30]. Overall, transmyocardial iontophoretic drug delivery was proven to be a more effective drug delivery technique than passive diffusion and IV administration.

1.5.5 Intraductal

Intraductal drug administration using iontophoresis offers a novel method to locally deliver chemotherapies to ductal carcinomas [32-33]. Komuro *et al*. developed an iontophoretic device that delivered the antiestrogen drug, miproxifen phosphate (TAT-59), and the active metabolite of TAT-59, dephosphorylated metabolite miproxifen (DP-TAT-59) through the nipple, directly into the mammary ducts. In *in vitro* rat skin studies, iontophoretic drug delivery, using 0.5 mA/cm^2 for two hours, was compared to passive diffusion. Using high performance liquid chromatography, TAT-59 concentrations were determined, affirming that iontophoretic delivery increased drug permeation into the ducts compared to passive diffusion, where TAT-59 penetration was hardly detectable. In a canine *in vivo* study by Komuro *et al*., iontophoretic delivery was compared to oral administration [32]. TAT-59 tissue concentrations were compared after 5 days of repeated iontophoretic delivery and 14 days after oral delivery, when the drug reached a steady state. The studies indicated that TAT-59 was delivered directly to the mammary tissues after iontophoretic delivery and TAT-59 drug levels were undetectable in the plasma. The area under the curve value of DP-TAT-59 was 3 times larger during iontophoresis than oral administration, indicating an increase in DP-TAT-59 delivery due to iontophoretic administration.

Iontophoretic devices to treat ductal carcinoma offer non-invasive routes of drug delivery that can be self-administered by patients. One drawback is that drug concentration within the tissues tends to vary between patients due to the biological and physiological differences [32]. Though the drug concentration still needs to be optimized, iontophoresis has the potential of increasing the efficacy of drug delivery to mammary ducts and tissues.

1.5.6 Intraluminal

The inefficiency of current percutaneous therapies for treating restenosis has led to the fabrication of an iontophoretic balloon to transport anti-restenotic drugs to vessel walls after angioplasty [34]. A balloon catheter consisting of an Ag/AgCl cathodal electrode wrapped around a catheter shaft and an anodal electrode placed on the skin was developed by CorTrak Medical, Inc,. The catheter was surrounded by a porous balloon with impermeable ends that is placed in contact with the vessel walls, allowing for increased localized drug delivery [35-37].

Studies have been conducted with the intention of optimizing anti-restenotic agent delivery to narrowed blood vessels, testing the pharmacokinetics and localization of coronary delivery [38]. Fernandez-Ortiz *et al.* conducted an *in vivo* study using an iontophoretic catheter to deliver ^{125}I-hirudin throughout the layers of the arterial wall [34]. In the porcine study, r-hirudin was transported to 20 arteries, 2 by means of passive diffusion and 18 by a 4 mA/cm^2 current density for 5 minutes. Drug levels due to the iontophoretic balloon catheter were 80 times higher than r-hirudin levels by passive diffusion. The drug levels in vessels declined rapidly, decreasing from a C_{max} of 0.78 μg g tissue^{-1} mm^{-1} by iontophoretic delivery to 0.14 μg g tissue^{-1} mm^{-1} after 1 hour and 0.02 μg g tissue^{-1} mm^{-1} after 3 hours. The vessels that received the drug through iontophoretic balloon catheter administration suffered only minimal damage by the device 48 hours after treatment. In another *in vivo* study conducted by Mitchel *et al.*, intravascular iontophoretic balloon catheters delivered heparin into the coronary arterial walls of 33 rats and 21 pigs [33]. Iontophoretic delivery in the rat studies delivered 13 times the levels of heparin than that of passive diffusion. In a study by Robinson *et al*., oligonucleotides were delivered to coronary arteries in pigs after angioplasty; there

was a detectable amount of the delivered oligonucleotide distributed throughout the arterial tissue that persisted for 7 days [38]. In a study by Markwart F *et al*., iontophoretically delivered dextran-bound hirudin displayed a tissue half-life of 7 hours compared to the short tissue half-life of r-hirudin (1-2 hours) [34,39]. Liposomes and microspheres are also under investigation for increasing the duration of drug levels, offering a possibility of delivering larger dosages of drugs at controlled rates [37]. Iontophoretic balloon catheters provide a non-invasive way to directly target angioplasty sites, delivering increased concentrations of anti-restenoic drugs, oligonucleotides, hirudin, and heparin into blood vessels.

1.6 Conclusion

The overview of iontophoretic drug delivery presented here illustrates that a considerable amount of effort has gone into exploring the feasibility of iontophoresis as a treatment platform for a number of therapeutic areas and many different drug molecules with diverse physicochemical properties. Overall, iontophoresis confers control over the drug input kinetics and the ability to customize drug input rates that can be optimized for a given patient.

1.7 REFERENCES

[1] B.H. Sage, J.E. Riviere. Model systems in iontophoresis – transport efficacy. Adv. Drug Del. Rev. 9, 265-287 (1992).

[2] A. Helmstadter. The history of electrically-assisted transdermal drug delivery. Pharmazie 56, 583-587 (2001).

[3] G.F. Pivati. Della electtricita medica lettera. Lucca 31 (1747).

[4] E.P. Cumberbatch. Essentials of Medical Electricity. 8th edition. London 1939.

[5] F. Krause. Elektromedizinische Werke, Preisliste Berlin 1905.

[6] J.N. Dyson. The practice of ionization. London 1936.

[7] C. Cullander, G. Rao, R.H. Guy. Why silver/silver chloride? Criteria for iontophoresis electrodes. Prediction Percutaneous Penetration 3B, 381-390 (1993).

[8] J.B. Phipps, R.V. Padmanabhan, G.A. Lattin. Iontophoretic delivery of model inorganic and drug ions. J. Pharm. Sci. 78, 365–369 (1989).

[9] B.H. Sage, J.E. Riviere, Model systems in iontophoresis—transport efficacy. Adv. Drug Deliv. Rev. 9, 265–287 (1992).

[10] Y.N. Kalia, A. Naik, J. Garrison, R.H. Guy. Iontophoretic drug delivery. Adv. Drug Deliv. Rev. 56, 619-658 (2004).

[11] M.J. Pikal, The role of electroosmotic flow in transdermal iontophoresis. Adv. Drug Deliv. Rev. 9, 201– 237 (1992).

[12] M.J. Pikal, Transport mechanisms in iontophoresis: I. A theoretical model for the effect of electroosmotic flow on flux enhancement in transdermal iontophoresis. Pharm. Res. 7, 118–126 (1990).

[13] M.J. Pikal, S. Shah, Transport mechanisms in iontophoresis: II. Electroosmotic flow and transference number measurements for hairless mouse skin. Pharm. Res. 7, 213–221 (1990).

[14] M.J. Pikal, S. Shah, Transport mechanisms in iontophoresis: III. An experimental study of the contributions of electroosmotic flow and permeability change in transport of low and high molecular weight solutes. Pharm. Res. 7, 222– 229 (1990).

[15] D. Marro, R.H. Guy, M.B. Delgado-Charro, Characterization of the iontophoretic permselectivity properties of human and pig skin. J. Control. Release 70, 213– 217 (2001).

[16] R.H. Guy, Y.N. Kalia, M.B. Delgado-Charro, V. Merino, A. Lopez, D. Marro, Iontophoresis: electrorepulsion and electroosmosis. J. Control. Release 64, 129–132 (2000).

[17] R.H. Guy. Interview with Richard H Guy by Hannah Coaker. Ther. Deliv. 5, 123-128 (2014).

[18] P.C. Kasha, A.K. Banga. A review of patent literature for iontophoretic delivery and devices. Recent Pat. Drug Deliv. Formul. 2, 41-50 (2008).

[19] E. Elijarrat-Binstock, A.J. Domb, Iontophoresis: A non-invasive ocular drug delivery. Journal of Controlled Release 110, 479-489 (2006).

[20] R. Grossman, D.F. Chu, D.A. Lee, Regional ocular gentamicin levels after transcorneal and transccleral iontophoresis. Investigative Ophthalmology & Visual Science 31, 909-916 (1990).

[21] E. Eljarrat-Binstock, F. Orucov, Y. Aldouby, J. Frucht-Pery, A.J. Domb, Charged nanoparticles delivery to the eye using hydrogel iontophoresis. Journal of Controlled Release 126, 156-161 (2008).

[22] Eyegate Pharmaceuticals, Inc, http://www.eyegatepharma.com, 2013.

[23] S.M. Di Stasi, C. Riedl, Updates in intravesical electromotive drug administration of mitomycin-C for non-muscle invasive bladder cancer. World J Urol 27, 325-330 (2009).

[24] S.M. Di Stasi, G. Vespasiani, A. Giannantoni, R. Massoud, S. Dolci, F. Micali, Electromotive delivery of mitomycinc C into human bladder wall. Cancer Res 57, 875–880 (1997).

[25] S.M. Di Stasi, A Giannantoni, R Massoud, S. Dolci, P. Navarra, G. Vespasiani, R.L. Stephen, Electromotive versus passive diffusion of mitomycin C into human bladder wall: concentration-depth profiles studies. Cancer Res, 59, 4912–4918 (1999).

[26] C.R. Riedl, M. Knoll, E. Plas, H. Pfluger, Intravesical electromotive drug administration technique: preliminary results and side effects. J Urol 159, 1851-1856 (1998).

[27] S.M. Di Stasi, A. Giannantoni, G. Arcangelo, M. Valenti, G. Zampa, L. Storti, F. Attisani, A. De Carolis, G. Capelli, G. Vespasiani, R.L. Stephen, Sequential BCG and electromotive mitomycin versus BCG alone for high-risk superficial bladder cancer: a randomized controlled trial. The Lancet Oncology 7, 43- 51 (2006).

[28] S.M. Di Stasi, A. Giannantoni, R.L. Stephen, G. Capelli, P. Navarra, R. Massoud, G. Vespasiani, Intravesical electromotive mitomycin C versus passive transport mitomycin C for high-risk superficial bladder cancer: a prospective randomized study. J Urol 170, 777-782 (2003).

[29] S. M. Di Stasi, L. Storti, A. Giurioli, G. Zampa, E. Liberati, M. Sciarra, B. Iorio, R.L Stephen, Carcinoma in situ of the bladder: long-term results of a randomized prospective study comparing intravesical electromotive mitomycin-C, passive diffusion mitomycin-C and Bacillus Calmette-Guerin. Eur Urol Suppl 7, 180 (2008).

[30] B. Avitall, J. Hare, G. Zander, C. Bockoff, P. Tchou, M. Jazayeri, M. Akhtar, Iontophoretic transmyocardial drug delivery. A novel approach to antiarrhythmic drug therapy. Circulation 85, 1582-1593 (1992).

[31] V. Labhasetwar, T. Underwood, S. Schwendeman, R. Levy, Iontophoresis for modulation of cardiac drug delivery in dogs. Proc. Natl. Acad. Sci. 92, 2612-2616 (1995).

[32] M. Komuro, K. Suzuki, M. Kanebako, T. Kawahara, T. Otoi, K. Kitazato, T. Inagi, K. Makino, M. Toi, H. Terada, Novel iontophoretic administration method for local therapy of breast cancer. Journal of Controlled Release 168, 298-306 (2013).

[33] S.M. Love, B. Zhang, W. Zhang, B. Zhang, H. Yang, J. Rao, Local drug delivery to the breast: a phase 1 study of breast cytotoxic agent administration prior to mastectomy. BMC Proc. 3, S29 (2009).

[34] A. Fernandez-Ortiz, B.J. Meyer, A. Mailhac, E. Falk, L. Badimon, J.T. Fallon, V. Fuster, J.H Chesebro, J.J. Badimon, A new approach for local intravascular drug delivery. Iontophoretic balloon. Circulation 89, 1518-1522 (1994).

[35] J.F. Mitchel, M.A. Azrin, D.B. Fram, L.M. Bow, R.G. McKaw, Localized Delivery of Heparin to Angioplasty Sites With Iontophoresis. Cathetherication and Cardiovascular Diagnosis 41, 315-323 (1997).

[36] R. Sachar, E.J. Topol, Local Gene and Cell Delivery Devices, Contemporary Cardiology: Essentials of Restenosis: For the Interventional Cardiologist 419-442 (2007).

[37] R.R. Makkar, N. Eigler, F. Litvack, J.S. Forrester, Prevention of Restenosis by Local Drug Delivery. Journal of Cardiovascular Pharmacology and Therapeutics, 1, 177-188 (1996).

[38] K. A. Robinson, N.A.F. Chronos, E. Schieffer, S.J. Palmer, G.D. Cipolla, P.G. Milner, R.G. Walsh, S.B King, Pharmacokinetics and Tissue Localization of Antisense Oligonucleotides in Balloon-Injured Pig Coronary Arteries After Local Delivery With

an Iontopheretic Balloon Catheter. Catheterization and Cardiovascular Diagnosis 41, 354-359 (1997).

[39] F. Markwardt, M. Richter, P. Walsmann, G. Riesener, M. Paintz, Preparation of dextran-bound recombitant girudin and its pharmacokinetic behavior. Biomad Biochem Acta., 29, 1103-1108 (1990).

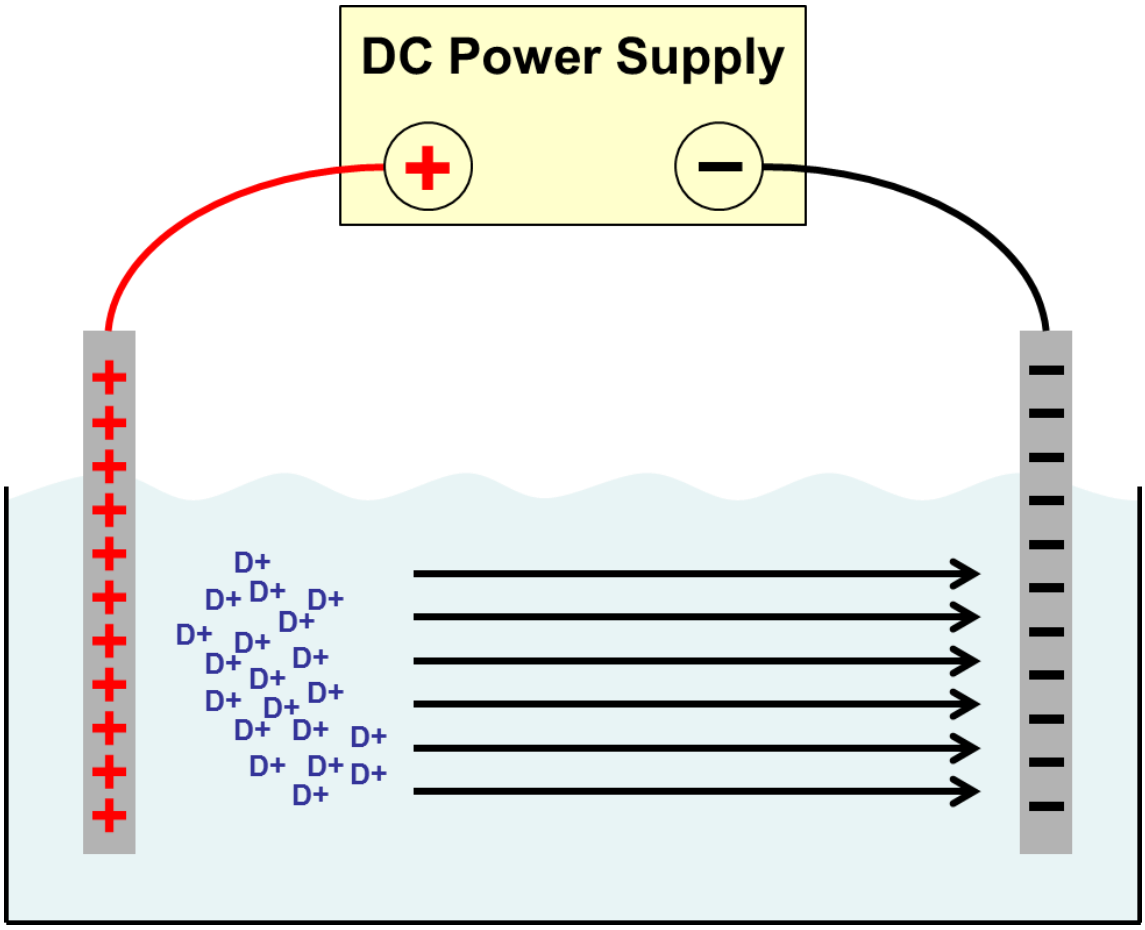

Figure 1.1. Model iontophoretic system involving a power source connected to two electrodes generating an electric current in a cationic drug solution.

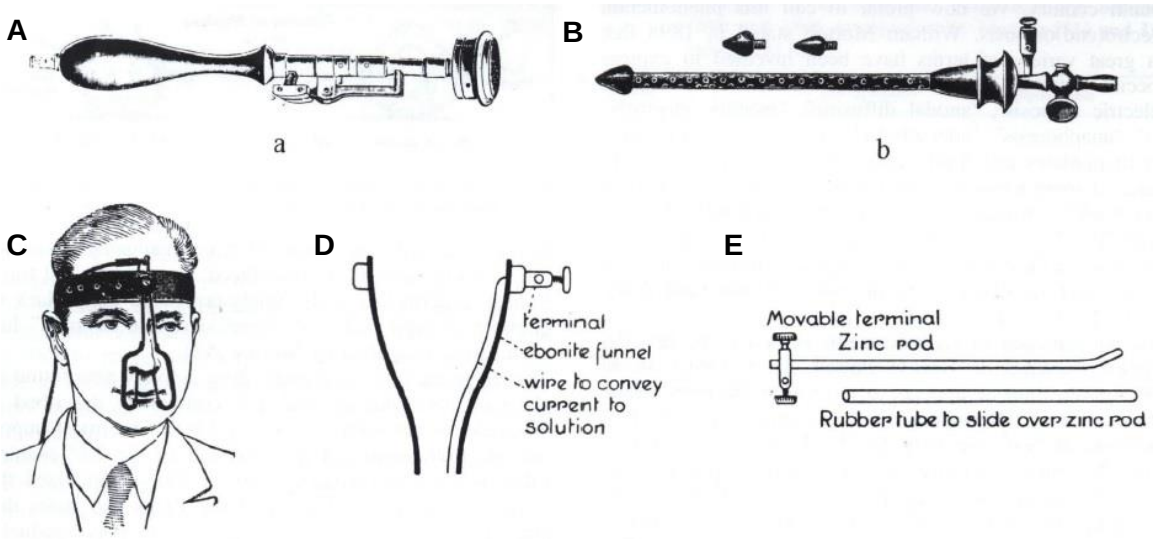

Figure 1.2. Different types of electrodes for iontophoretic drug delivery. (A) Diffusion electrode according to Adamkiewicz, (B) electrode for urethral iontophoresis, (C) electrode according to Franklyn for treating hay fever by zinc ionization, (D) vulcanite funnel electrode for ionization of the mucous membrane of the middle ear, (E) zinc rod electrode used for ionization of the mucous membrane of canal or cervix uteri [4-6].

Inert electrodes: e.g., carbon or platinum electrodes

$2\ H_2O \rightarrow 4H^+ + O_2 + 4\ e^-$ (at anode)

$2\ H_2O + 2\ e^- \rightarrow H_2 + 2HO^-$ (at cathode)

Reversible electode: e.g., Ag/AgCl electrodes

$Ag \rightarrow Ag^+ + e^- \rightarrow AgCl + e^-$ (at anode)

$AgCl + e^- \rightarrow Ag + Cl^-$ (at cathode)

Figure 1.3. Electrochemistry of commonly used electrodes for iontophoretic drug delivery.

$$J_X^T = J_X^{EM} + J_X^{EO}$$

Equation 1.1. Total iontophoretic flux.

$$J_X^{EM} = \frac{1}{z_X AF} \cdot i_X$$

Equation 1.2. Electromigratory flux of an ion, X, is related to the component current flow i_X due to its transport by Faraday's constant, F.

$$J_X^{EM} = \frac{1}{z_X AF} \cdot t_X I$$

Equation 1.3. Electomigratory flux according to applied current, I, and a proportionality constant, t_X.

$$J_X^{EM} = \left(\frac{1}{z_X F}\right) \frac{z_X u_X c_X}{\sum_{n=0}^{i} z_i u_i c_i} \cdot I_D$$

Equation 1.4. Electomigratory flux of ion X in the presence of other charge carriers.

$$\text{Volume flow} = L_{11}\Delta\text{Pressure} + L_{12}(-\Delta\text{Potential})$$

$$\text{Current flow} = L_{21}\Delta\text{Pressure} + L_{22}(-\Delta\text{Potential})$$

Equation 1.5. Current and volume flows resulting from the application of pressure and potential differences across a membrane.

$$\frac{\text{Volume flow}}{\text{Current flow}} = \frac{L_{12}}{L_{22}} = \text{electroosmotic flow}$$

Equation 1.6. Electroosmotic flow is the result of volume flow induced by the current flow.

$$J_X^T = J_X^{EM} + J_X^{EO} = \left(\frac{1}{z_X F}\right) \frac{z_X u_X c_X}{\sum_{n=0}^{i} z_i u_i c_i} \cdot I_D + v c_X$$

Equation 1.7. Total iontophoretic flux of a cationic drug.

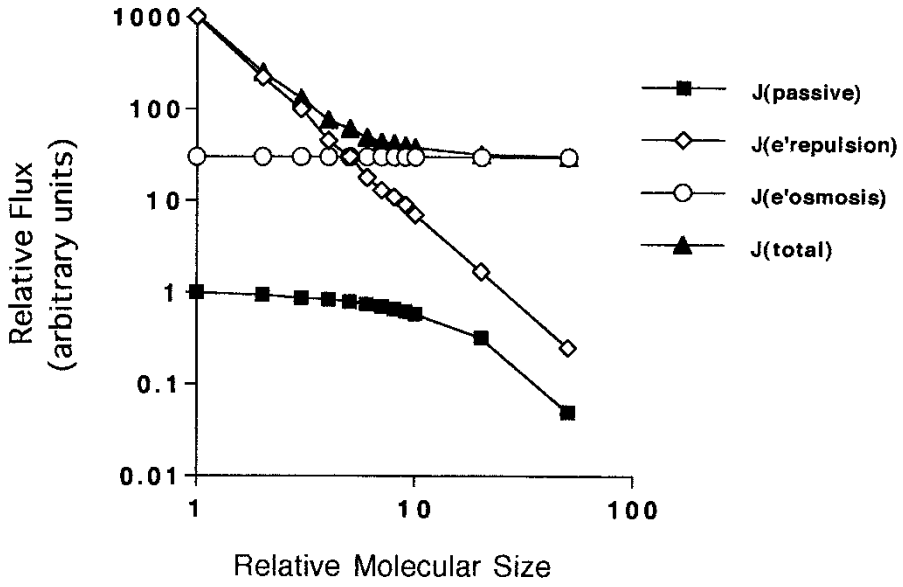

Figure 1.4. Relative ion flux as a function of molecular size [16].

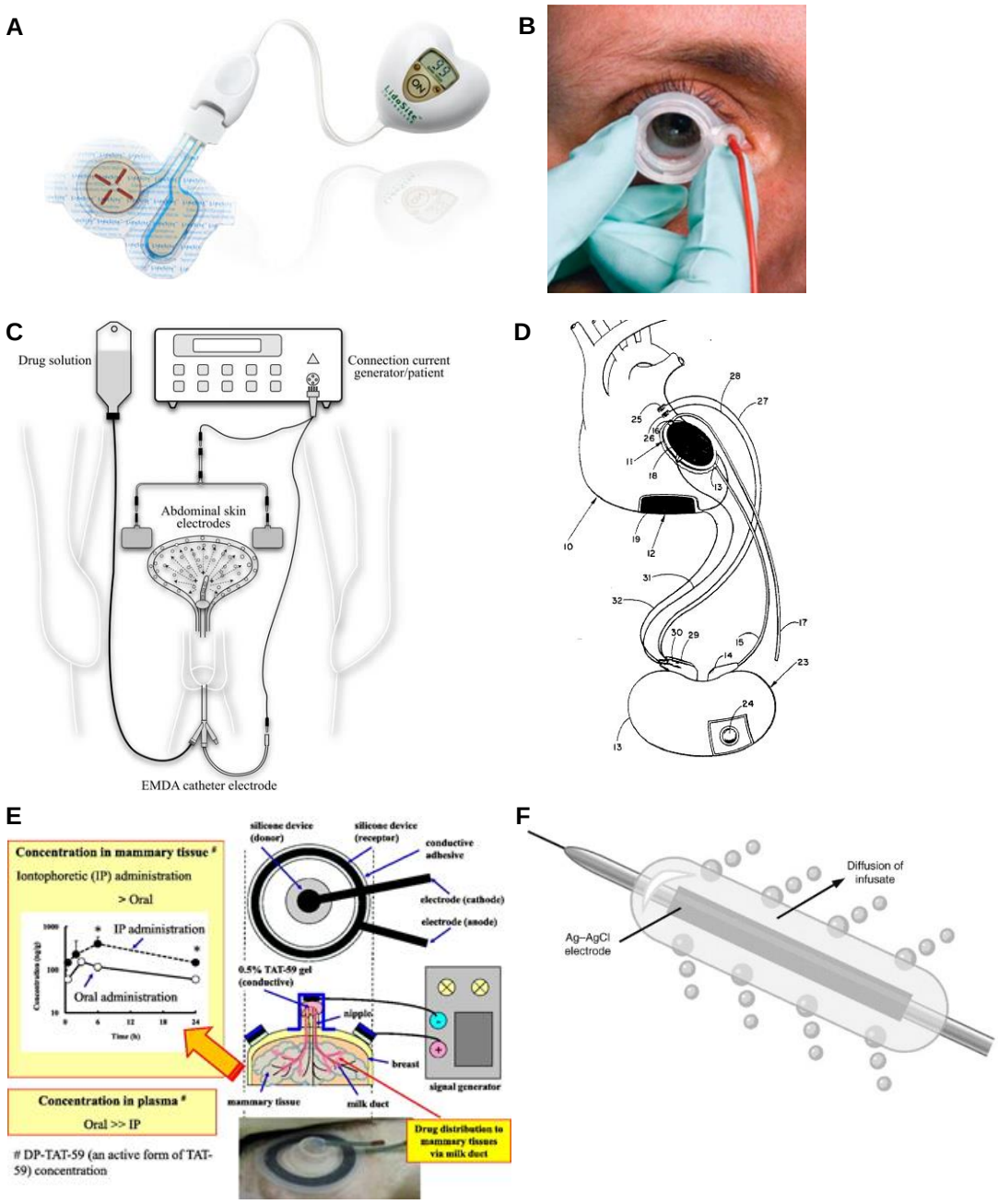

Figure 1.5. Iontophoretic devices for local drug delivery. (A) Lidosite for the transdermal delivery of lidocaine [10]. (B) Eyegate II delivery system for ocular iontophoresis to the anterior and posterior of the eye [22]. (C) EMDA device used to locally deliver MMC to bladder cancer [23]. (D) Transmyocardial iontophoretic device for delivery of anti-arrhythmic drugs [30]. (E) Intraductal delivery of an anti-estrogen drug for ductal carcinomas in situ [32]. (F) Coronary artery iontophoretic balloon catheter for delivery of anti-restenotic drugs [37].

CHAPTER 2: LOCAL IONTOPHORETIC ADMINISTRATION OF GEMCITABINE FOR THE TREATMENT OF PANCREATIC CANCER

2.1 Overview

With an incidence rate approximately equivalent to the death rate, pancreatic cancer is the fourth leading cause of cancer death in the United States. The poor prognosis is in part attributed to the ineffective delivery of chemotherapeutics. Poor tissue perfusion plays a substantial role in preventing adequate drug accumulation in primary pancreatic tumors. In an attempt to address the ineffectiveness of systemically administered gemcitabine, we have developed modalities for the localized delivery of cytotoxic chemotherapies to pancreatic tumors. These devices utilize an applied electric field to drive chemotherapeutics into the tumor. Device treatments were performed in patient-derived xenograft mouse models of pancreatic cancer and a non-tumor bearing canine model. We demonstrate that local iontophoretic delivery of gemcitabine results in enhanced drug accumulation, penetration, and efficacy compared to IV administration.

2.2 Introduction

In 2014, it is estimated that 46,420 new cases of pancreatic cancer will be diagnosed and 39,590 individuals will die from pancreatic cancer in the United States. The 1-year and 5-year relative survival rates for all stages are 24% and 5%, respectively [1,2]. Surgical resection offers the only cure, but only 20% of patients have resectable disease at the time of

diagnosis. Approximately 40% of patients have metastatic disease and another 40% have locally advanced unresectable tumors [3].

Systemic control of pancreatic cancer has been the primary emphasis in research efforts, yet local control rates of this disease remain poor. Local symptoms of pancreatic tumors can cause substantial morbidity and decreased quality of life, suggesting a dire need for an adjunct to surgery and palliative care of this devastating cancer. Systemically delivered gemcitabine and other chemotherapies have been suggested to be ineffective in the local control of pancreatic cancer because of impaired drug delivery [4]. Poor tissue perfusion plays a substantial role in preventing adequate drug exposure to primary pancreatic tumors [4-9]. For this reason, we have proposed to employ an iontophoretic approach to drive increased amounts of chemotherapeutics deep into the primary tumor [10]. In the area of oncology, iontophoretic techniques have been successfully translated to the treatment of bladder cancers in the delivery of mitomycin C [10-12].

Herein, we describe the first iontophoretic device for the local delivery of a cytotoxic chemotherapy to pancreatic tumors. This use of an applied electric potential for local delivery of chemotherapies offers the capability of overcoming the considerable flow and pressure gradients seen in pancreatic tumors. Overall, this device potentially offers an entirely new modality for the treatment of pancreatic cancer under the emerging field of interventional oncology. Moreover, the further development of these devices could translate directly into new treatments for other types of primary tumors and metastatic diseases.

2.3 Results

2.3.1 Device Design and Proof-of-Concept Testing

Our devices were designed to adapt conventional iontophoretic drug delivery techniques. Figure 2.1A-C showcases the device, the assembly, and the setup for animal treatments. The devices primarily consisted of (i) an electrode in direct contact with the drug solution, (ii) a polyurethane reservoir surrounding the electrode, and (iii) an inlet and outlet for continuous drug flow through the reservoir. This continuous drug flow maintained a constant drug concentration around the electrode and pressure within the device. Under an applied electric potential, the drug was transported in the direction normal to the electrode and into the tissue.

A number of device parameters were evaluated to determine the optimal drug transport conditions from the device, including drug influx rates (Figure 2.1D), electrode material (Figure 2.1E), currents applied (Figure 2.1F), and drug concentration (Figure 2.1G). We found that drug influx at 50 μL/min or greater resulted in the largest amount of gemcitabine delivered into tissue surrogates (2 wt% agarose gels) at 2 mA while maintaining a low voltage ($P = 0.006$) (Figure 2.1D). Two mA was the maximum current allowed without impacting the integrity of the device. A number of conducting materials with diverse electrochemical properties for the device anode were evaluated, including platinum, silver, and poly(3,4-ethylenedioxythiophene) (PEDOT). We found that silver was the most efficient material for drug transport into tissue surrogates ($P = 0.03$) (Figure 2.1E). However, the electrochemical reaction at the silver anode interface prohibited its long-term use due to the buildup of silver chloride. Platinum was chosen for long-term implanted device studies, while silver was used for short-term non-implanted device studies. The application of 2 mA

of current resulted in 1.44-fold greater drug transport compared to 1 mA of current (P = 0.056) (Figure 2.1F). Lastly, the transport of three concentrations of gemcitabine, 40, 20, and 10 mg/mL, into tissue surrogates using a 2 mA constant current applied for 10 minutes resulted in significantly large differences in drug transport (P = 0.0001 for 40 vs 20 mg/L gemcitabine and P = 0.0004 for 20 vs 10 mg/mL gemcitabine) (Figure 2.1G). In addition to optimizing device functionality, testing these parameters on tissue surrogates gave us a preliminary idea of the drug transport capability.

2.3.2 Drug Transport in Human Tissue

Ex vivo drug transport studies were conducted using pancreatic cancer patient-derived xenografts (PDXs). To test the transport of gemcitabine in the ex vivo PDX tumors, the devices were sutured onto the tumors and the counter electrode placed on the contralateral side of the tumor. Two or 0 mA of current was applied for 10 minutes, and the tumors were subsequently snap frozen, processed, and analyzed by UV-high performance liquid chromatography (HPLC). The application of current resulted in a 9.1-fold increase in drug transport when current was applied compared to the passive diffusion control (current = 0 mA) (Figure 2.2).

2.3.3 Pharmacokinetic Studies in a PDX Pancreatic Cancer Model

Iontophoretic delivery of gemcitabine was further characterized with respect to pharmacokinetics (PK) in an orthotopic PDX model of pancreatic cancer. Recent reports in lung, pancreatic, breast and colon cancers, as well as glioblastomas, suggest that patient tumors directly implanted in immune-compromised mice exhibit response rates to cytotoxic

or targeted therapies more similar to patient responses [13-16]. These tumors retain the heterogeneity and histological characteristics of the original patient tumors. In the PDX model, devices were surgically implanted when the tumor reached a median size of ~260 mm^3, as determined by high-resolution 3D ultrasound that correlated very well with volume displacement. Mice were allowed to recover for a week after device implantation. A single treatment was administered and tumors were harvested at designated time points. Figure 2.3 shows a typical PK study for the device delivery of gemcitabine compared to IV delivery (80 mg/kg). Gemcitabine plasma exposure as measured by the area under the curve (AUC) for IV delivery was 65.2 hr*µg/mL, with no detectable gemcitabine in the plasma of the device arm. Furthermore, gemcitabine tumor AUC for iontophoretic delivery and IV delivery were 384.1 and 30.8 hr*µg/g, respectively. The average distances that gemcitabine was detected in the tumors in the direction away from the devices were 4.7 mm at 0 hours and 3 mm at 3 and 6 hours; for IV gemcitabine-treated mice, gemcitabine was detected throughout the entirety of the tumor but at significantly lower drug concentrations. Additionally, single time point PK of the device delivery of high (40 mg/mL) or low (10 mg/mL) gemcitabine concentrations (n=3, each) was evaluated directly after treatment revealing 11.6-fold and 2.4-fold higher amounts of gemcitabine in the tumor and significantly lower plasma exposure compared to IV delivery. The average distances that gemcitabine was detected in the tumors in the direction away from the devices were 5.0 mm for the high gemcitabine concentration and 3.7 mm for low gemcitabine concentration. We observed that the drug accumulation in the tumor and distance of drug transport was dependent upon the influx gemcitabine concentration, which correlated with the in vitro drug transport results.

2.3.4 Device Efficacy

To evaluate the antitumor activity of gemcitabine delivered by the iontophoretic devices, we performed efficacy studies in an orthotopic PDX pancreatic cancer model. Devices were surgically implanted onto orthotopic PDX tumors when their size reached ~260 mm^3, as determined by high-resolution 3D ultrasound. Mice were treated twice a week for up to 7 weeks with device gemcitabine (20 mg/mL), device saline (0.9% NaCl), IV gemcitabine (80 mg/kg), or IV saline. Implanted devices impaired ultrasound imaging, and thus, tumor volumes were measured by volume displacement only after completion of the scheduled treatment. Device gemcitabine resulted in significant tumor regression in 7 of 7 mice, outperforming IV gemcitabine and the control arms of IV and device saline over the 52-day period of the study (Figure 2.4). Mice treated with device gemcitabine had a mean log_2-fold change in tumor volume of -0.8 compared to a mean log_2-fold change in tumor volume of 1.1 for IV gemcitabine ($P < 0.0001$), 3.0 for IV saline ($P < 0.0001$), and 2.6 for device saline groups ($P < 0.0001$). Mice treated with device saline had tumor volumes that were not statistically different from mice treated with IV saline. Device gemcitabine was better tolerated based on greater body weight gain compared to IV gemcitabine with minimal changes in alanine transaminase, aspartate transaminase, blood urea nitrogen (BUN), and lipase. Overall, device gemcitabine resulted in tumor regression in 7/7 mice compared to no regression (0/7) in the IV gemcitabine group while maintaining low systemic exposure of gemcitabine. Histological samples from the tumors post-treatment revealed a decrease in stain for a marker of cell proliferation, Ki-67, from device gemcitabine-treated mice compared with tumors from mice that received IV gemcitabine, IV saline, or device saline.

2.3.5 PK in Dogs

To further evaluate the implantable iontophoretic device, a representative large animal model for humans was used. However, since there was no readily available large animal model for pancreatic cancer, a non-tumor bearing canine model was chosen. A laparotomy was performed to expose the pancreas, and devices (Figure 2.5A) were sutured directly onto the pancreas. A constant current of 10 mA was applied for 60 minutes using either 40 or 10 mg/mL gemcitabine (n = 5 per group). For the IV treatment arm (n = 4, per group), clinical protocol was followed for gemcitabine administration, which was an infusion of a 1 g/m^2 dose for 30 minutes, and the animal was euthanized 60 minutes after the start of the infusion. The plasma was sampled at 15 minute increments before, during, and after therapy (Figure 2.5B). After therapy, the tissues were subsequently removed, flash-frozen, and analyzed by UV-HPLC. There was no drug detected in the plasma of the animals at any time when a low gemcitabine concentration (10 mg/mL) was used in the device treatment. In the plasma of dogs treated with the high gemcitabine concentration (40 mg/mL) delivered by the device, 2 of 5 dogs had detectable levels of gemcitabine, but the levels of gemcitabine detected were at least 25-fold less than the IV treatment ($p < 0.0001$). Gemcitabine was detected in the plasma of all dogs that received IV gemcitabine. There was a 7.1- and 2.0-fold increase in the concentration of gemcitabine in the normal canine pancreas after device delivery using high ($p = 0.0002$) and low ($p = 0.42$) gemcitabine concentrations, respectively, compared to IV administration (Figure 2.5C). The distance of gemcitabine transport after device treatment using high and low gemcitabine concentrations were statistically different ($p = 0.03$) at 9.6 mm and 6.3 mm away from the electrode, respectively (Figure 2.6D).

2.4 Discussion

Novel therapeutic strategies, such as local drug delivery devices, are critical for the improvement of pancreatic cancer treatments. Local delivery of chemotherapeutic agents allows for an increase in the concentration of the drug in the area of greatest need, while limiting systemic side effects of IV and orally administered chemotherapeutic agents. However, relatively few methods have been developed for the local delivery of chemotherapeutic agents for pancreatic cancer. Tanaka and colleagues have generated a method for the temporary unification of the pancreatic blood supply for advanced pancreatic cancer, which enhances regional drug delivery into the pancreas and liver [17]. Furthermore, interventional endoscopic ultrasound enables the use of radiofrequency ablation and injection of anti-cancer agents, such as ONYX-015 and TNFerade™ [18].

The results from our *in vivo* device studies suggest the opportunity for improved and effective local delivery of gemcitabine and other cytotoxic therapies for the treatment of pancreatic cancer. Gemcitabine has a short half-life in the systemic circulation of humans, which is similar to the canine model where gemcitabine has a half-life of 1.38 hours [19]. The rapid metabolism of gemcitabine in the plasma can be overcome by local drug delivery. Our data indicate that significant amounts of gemcitabine can be transported in the local region surrounding the devices when a constant current is applied. Systemic exposure after device delivery is extremely low, and in many of our studies, not quantifiable. Furthermore, the device configurations that were evaluated prove the use of a clinically relevant electrode system for the iontophoretic delivery of gemcitabine.

Currently, the only cure for pancreatic cancer is resection of the primary tumor lesions. Approximately 80% of patients are considered ineligible for surgical resection

because the tumor has either invaded critical vessels or metastasized to more distant organs [20]. Our device has the potential to be a neoadjuvant therapy that may help convert the 40% of patients with tumors that are unresectable but not metastatic to surgical candidates. The device's ability to increase intratumoral drug concentrations well above current methods of drug administration, while maintaining low systemic exposure, can increase rates of tumor regression and margin-negative surgical resection. For patients with metastatic disease and debilitating local symptoms such as pancreaticobiliary and gastric outlet obstruction, this device can provide a palliative modality to improve symptom control. Moreover, this therapy could be used as an adjunct treatment to systemically administered therapy, in order to treat primary and metastatic tumors lesions. One tremendous advantage would be to leverage our device for the delivery of agents that are limited by systemic toxicity. For example, FOLFIRINOX is a promising cytotoxic combination but with limited utility in many patients due to its high level of systemic toxicity [21]. Therefore, device delivery of FOLFIRINOX would have the potential to substantially improve the resectability and local control rate in patients with locally advanced and unresectable pancreatic cancer.

Our devices could potentially offer entirely new modalities for the treatment of pancreatic cancer under the emerging field of interventional oncology. We further anticipate this being a platform technology that will translate directly into the treatment of other cancers including the chest recurrence of breast cancer and head and neck, esophageal, and colorectal cancers.

2.5 Materials and Methods

2.5.1 Design and Fabrication of Device

Iterative device design was performed using the 3D computer-aided design software, SolidWorks. The devices were fabricated according to a reservoir-based design. For the murine device, a polyurethane reservoir was fabricated with a stainless steel wire ring embedded to allow for suturing of the device to the tumor. A platinum disc was soldered to a stainless steel cable wire and embedded in the reservoir. The electrode wire was threaded through the multi-luminal tubing. A semipermeable cellulose membrane was adhered to the casing to enclose the reservoir. For the canine device, a polyethylene reservoir was fabricated, and one side of a 1 cm silver circular electrode was soldered to an insulated copper conducting wire. Press-molding was used to attach a semi-permeable cellulose membrane, which was situated parallel to the silver electrode to allow for drug transport into the tissue from the reservoir. A dual luminal tube was inserted into the reservoir for drug flow into and out of the reservoir. A nylon mesh was adhered by Dymax UV cure adhesive to the back of the pressurized anode. For the cathode on the back of the murine model, a 1 cm silver chloride disc was used. For the cathode on the back of the canine model, a 5x7 inch electrocautery plate was used.

2.5.2 PDX Model of Pancreatic Cancer

Under IRB approval and according to IACUC guidelines, de-identified tumors of pancreatic cancer patients were grafted and passaged into immunocompromised mice as previously described [22]. Devices were surgically implanted on to the subcutaneous flank tumor once tumors reached an average size of 260 mm^3 volume. Gemcitabine was

formulated at 40, 20, and 10 mg/mL concentrations by diluting gemcitabine hydrochloride (APP Pharmaceuticals, LLC) powder in normal saline. A constant direct current (DC) power supply was used to provide 2 mA current to the device. The positive lead was connected to the device wire, and the negative lead was connected to the counter electrode placed on the mouse's skin. A syringe pump was used to circulate the gemcitabine solution through the device at a flow rate of 10 µL/min over a period of 10 minutes. When the device was powered, drug was driven from the device reservoir, through the membrane and into the tumor tissue following the path of the electrical current. Upon completion of the treatment, the device was emptied of drug solution. For PK studies, terminal bleeds were performed. The tissue and device were extracted and snap frozen with liquid nitrogen and stored at -80 °C. Tetrahydrouridine (THU) solution (Calbiochem) was added to the blood, and the blood was centrifuged at 11,000 rpm for 10 minutes. The plasma was collected and stored at -80 °C. For the IV treatment arm of the study, mice were given a single dose of gemcitabine at 80 mg/kg, and the tissue was removed ten minutes post-infusion. For efficacy studies, the mice were treated up to 6 weeks using device with 40 mg/mL gemcitabine concentration, device with normal saline (0.9% NaCl), or IV gemcitabine (80 mg/kg).

2.5.3 Testing in Canine Model

The canine model was housed at Synecor LLC and treated according to Synecor IACUC protocol. The dogs weighed between 20-23 kilograms and were between 1-2 years old. The dogs were anesthetized, and the abdomen was shaven and cleaned prior to surgery. A laparotomy was performed, and the right lobe of the canine pancreas was exposed. The devices were implanted on the pancreas, ensuring good contact with the tissue. The device

was attached to a power supply, with the positive output attached to the wire connected to the silver electrode and the negative output attached to the cathode. A 5”x7” electrocautery patch was used as the cathode and was covered with gel and placed onto the back of the animal. A 1-gram vial of Gemzar® (Eli Lilly) was solubilized in 25 mL of saline, and the 25 mL was diluted to 100 mL (pH between 4 and 5). Using an IV infusion pump, the solution was pumped through the device at a flow rate of 1.5 mL/min over a period of 60 minutes. Upon drug flow through the device, a constant current of 10 mA was applied for 60 minutes. 10mL of blood was sampled at 15 minutes increments prior to and during therapy and collected into heparinized tubes with 40 µL of a 10 mg/mL tetrahydrouridine (THU) solution. Upon completion of the 60 minutes, the device was emptied of drug solution. The dogs were euthanized with potassium chloride solution, and the tissue and device were extracted and snap frozen with liquid nitrogen and stored at -80 °C. The blood was centrifuged at 2,000 rpm for 10 minutes, and the plasma was collected and stored at -80 °C.

2.5.4 Processing of Tissue and Plasma

The frozen tissue was sectioned by a Leica cryostat microtome at -20 °C. The tissue was sectioned at 50 µm increments up to one centimeter away from the electrode. Frozen tissue sections were combined to reduce the sample number. To the specimens, the internal standard, 2’dC, was added at a concentration of 20 µg/mL. To the specimens, 0.08 mg/mL THU, 0.4 M perchloric acid solution was added at a liquid to mass ratio of 3:1 (v/w). The samples were vortexed and sonicated in an ice bath for 10 minutes. The samples were centrifuged at 4,000 rpm for 10 minutes, the pellet was washed with 0.4 M perchloric acid and centrifuged again at 4,000 rpm for 10 minutes, and the supernatants were combined.

Potassium hydroxide was added to bring the pH to 3 and the insoluble salt, potassium perchlorate, was removed by centrifugation. The supernatant was analyzed by UV-HPLC. To the plasma samples, 2'dC was added for a concentration of 20 μg/mL. 2.0 M perchloric acid was added to the sample at 10 %v/v of the sample. The samples were vortexed, incubate on ice for 15 minutes, and centrifuged at 16,000 rpm at 4 °C for 10 minutes. Potassium hydroxide was added to bring the pH to 3 and the insoluble salt, potassium perchlorate, was discarded. A portion of the solution was analyzed by UV-HPLC.

2.5.5 UV-High Performance Liquid Chromatography Assay

An Agilent 1200 UV-HPLC was used to quantify the amount of drug in the sectioned tissue. An isocractic method using a mobile phase of 90% aqueous buffer (50.0 mM sodium phosphate and 3.0 mM sodium octyl sulfate) and 10% acetonitrile brought to pH 2.9 with o-phosphoric acid, which was developed from Kirstein and colleagues [23]. The stationary phase was a Waters Spherisorb ODS2 4.6x250 mm column. The internal standard, 2'dC, and gemcitabine were detected at 267 nm, and the run time for the UV-HPLC assay was 15 minutes. The peaks areas were integrated, and the concentration of gemcitabine was determined by reference to validated calibration curves. The calibration curves were created by plotting known concentrations of gemcitabine to the ratio of the absorbance of gemcitabine to the absorbance of the internal standard. For assay validation, two calibrations curves were created each day for three days with six series of quality control standards for each calibration curve.

2.5.6 Statistical Analysis

Wilcoxon Rank Sum tests were used to obtain sample size numbers for the canine experiments. As the data were normally distributed, t-tests were used for statistical analysis of data.

2.6 Additional Support

We would like to thank Xianxi Wang, Charlene Santos, Silvia Gabriela Herrera-Loeza, Mark Urtz, UNC animal studies core, PDX program, and tissue procurement facility for their contributions to this work. This work was supported by funding from the University Cancer Research Fund, Synecor LLC, Liquidia Inc., and an NIH Pioneer Award.

2.7 REFERENCES

[1] American Cancer Society. Cancer Facts & Figures 2013. Atlanta: American Cancer Society; 2013.

[2] A. Jemal, R. Siegel, E. Ward, Y. Hao, J. Xu, T. Murray, M.J. Thun. Cancer Statistics, 2008. CA Cancer J Clin 58, 71-96 (2008).

[3] D. Li, K. Xie, R. Wolff, J.L. Abbruzzese. Pancreatic Cancer. The Lancet 363, 1049-1057 (2004).

[4] K.P. Olive, M.A. Jacobetz, C.J. Davidson, A. Gopinathan, D. McIntyre, D. Honess, B. Madhu, M.A. Goldgraben, M.E. Caldwell, D. Allard, K.K. Frese, G. Denicola, C. Feig, C. Combs, S.P. Winter, H. Ireland-Zecchini, S. Reichelt, W.J. Howat, A. Chang, M. Dhara, L. Wang, F. Rückert, R. Grützmann, C. Pilarsky, K. Izeradjene, S.R. Hingorani, P. Huang, S.E. Davies, W. Plunkett, M. Egorin, R.H. Hruban, N. Whitebread, K. McGovern, J. Adams, C. Iacobuzio-Donahue, J. Griffiths, D.A. Tuveson. Inhibition of Hedgehog Signaling Enhances Delivery of Chemotherapy in a Mouse Model of Pancreatic Cancer. Science 324, 1457-1461 (2009).

[5] A.I. Minchinton, I.F. Tannock, Drug Penetration in Solid Tumors. Nat Rev Cancer 6, 583-592 (2006).

[6] P. Olson, D. Hanahan. Cancer. Breaching the Cancer Fortress. Science 324, 1400-1401 (2009).

[7] I.F. Tannock, C.M. Lee, J.K. Tunggal, D.S. Cowan, M.J. Egorin. Limited penetration of anticancer drugs through tumor tissue: a potential cause of resistance of solid tumors to chemotherapy. Clin Cancer Res 8, 878 (2002).

[8] M. Erkan, S. Hausmann, C.W. Michalski, A.A. Fingerle, M. Dobritz, J. Kleeff, H. Friess. The Role of Stroma in Pancreatic Cancer: Diagnostic and Therapeutic Implications. Nature Reviews Gastroenterology & Hepatology 9, 454-67 (2012).

[9] M. Yu, I.F. Tannock. Targeting Tumor Architecture to Favor Drug Penetration: A New Weapon to Combat Chemoresistance in Pancreatic Cancer? Cancer Cell 21: 327-329 (2012).

[10] S.M. Di Stasi, A. Giannantoni, R. Massoud, S. Dolci, P. Navarra, G. Vespasiani, R.L. Stephen. Electromotive versus Passive Diffusion of Mitomycin C into Human Bladder Wall: Concentration-Depth Profile Studies. Cancer Res 59, 4912-4918 (1999).

[11] S.M. Di Stasi, A. Giannantoni, A. Giurioli, M. Valenti, G. Zampa, L. Storti, F. Attisani, A. De Carolis, G. Capelli, G. Vespasiani, R.L. Stephen. Sequential BCG and

electromotive mitomycin versus BCG alone for high-risk superficial bladder cancer: a randomised controlled trial. Lancet Oncology 7, 43-51 (2006).

[12] S.M. Di Stasi, C. Riedl. Updates in Intravesical Electromotive Drug Administration of Mitomycin-C for Non-Muscle Invasive Bladder Cancer. World J Urol 27, 325-350 (2009).

[13] I. Fichtner, J. Rolff, R. Soong, J. Hoffmann, S. Hammer, A. Sommer, M. Becker, J. Merk. Establishment of patient-derived non-small cell lung cancer xenografts as models for the identification of predictive biomarkers. Clin Cancer Res. 14, 6456-6468 (2008).

[14] A.C. Kimmelman, A.F. Hezel, A.J. Aguirre, H. Zheng, J.H. Paik, H. Ying, G.C. Chu, J.X. Zhang, E. Sahin, G. Yeo, A. Ponugoti, R. Nabioullin, S. Deroo, S. Yang, X. Wang, J.P. McGrath, M. Protopopova, E. Ivanova, J. Zhang, B. Feng, M.S. Tsao, M. Redston, A. Protopopov, Y. Xiao, P.A. Futreal, W.C. Hahn, D.S. Klimstra, L. Chin, R.A. DePinho. Genomic alterations link Rho family of GTPases to the highly invasive phenotype of pancreas cancer. Proc Natl Acad Sci U S A 105, 19372-19377 (2008).

[15] B. Rubio-Viqueira, A. Jimeno, G. Cusatis, X. Zhang, C. Iacobuzio-Donahue, C. Karikari, C. Shi, K. Danenberg, P.V. Danenberg, H. Kuramochi, K. Tanaka, S. Singh, H. Salimi-Moosavi, N. Bouraoud, M.L. Amador, S. Altiok, P. Kulesza, C. Yeo, W. Messersmith, J. Eshleman, R.H. Hruban, A. Maitra, M. Hidalgo. An in vivo platform for translational drug development in pancreatic cancer. Clin Cancer Res 12, 4652-4661 (2006).

[16] J.J. Tentler, A.C. Tan, C.D. Weekes, A. Jimeno, S. Leong, T.M. Pitts, J.J. Arcaroli, W.A. Messersmith, S.G. Eckhardt. Patient-derived tumor xenografts as models for oncology drug development. Nature Reviews Clinical Oncology 9, 338-350 (2012).

[17] T. Tanaka, M. Sho, H. Nishiofuku, H. Sakaguchi, Y. Inaba, Y. Nakajima, K. Kichikawa. Unresectable pancreatic cancer: Arterial embolization to achieve a single blood supply for intraarterial infusion of 5-fluorouracil and full-dose IV gemcitabine. American Journal of Roentgenology 198, 1445-1452 (2012).

[18] R. Ashida, K.J. Chang. Interventional EUS for the treatment of pancreatic cancer. J Hepatobiliary Pancreat Surg 16, 592-597 (2009).

[19] L.A. Shipley, T.J. Brown, J.D. Cornpropst, M. Hamilton, W.D. Daniels, H.W. Culp. Metabolism and disposition of gemcitabine, and oncolytic deoxycytidine analog in mice, rats, and dogs. Drug Metab Dispos 20, 849-855 (1992).

[20] S. Gillen, T. Schuster, C. Meyer Zum Büschenfelde, H. Friess, J. Kleeff. Preoperative/neoadjuvant therapy in pancreatic cancer: a systematic review and meta-analysis of response and resection percentages. PLoS Med 20, 7 (2010).

[21] T. Conroy, F. Desseigne, M. Ychou, O. Bouché, R. Guimbaud, Y. Bécouarn, A. Adenis, J.L. Raoul, S. Gourgou-Bourgade, C. de la Fouchardière, J. Bennouna, J.B. Bachet, F. Khemissa-Akouz, D. Péré-Vergé, C. Delbaldo, E. Assenat, B. Chauffert, P. Michel, C. Montoto-Grillot, M. Ducreux; Groupe Tumeurs Digestives of Unicancer; PRODIGE Intergroup. FOLFIRINOX versus Gemcitabine for Metastatic Pancreatic Cancer. N Engl J Med. 364, 1817-25 (2011).

[22] J.E. Streeter, S.G. Herrera-Loeza, N.F. Neel, J.J. Yeh, P.A. Dayton. A Comparative Evaluation of Ultrasound Molecular Imaging, Perfusion Imaging, and Volume Measurements in Evaluating Response to Therapy in Patient-Derived Xenografts. Technol Cancer Res Treat. 12, 311-21 (2013).

[23] M.N. Kirstein, I. Hassan, D.E. Guire, D.R. Weller, J.W. Dagit, J.E. Fisher, R.P. Remmel. High performance liquid chromatographic method for the determination of gemcitabine and 2',2'-difluorodeoxyuridine in plasma and tissue culture media. J. Chromatogr. B Analyt. Technol. Biomed. Life Sci. 835, 136-142 (2006).

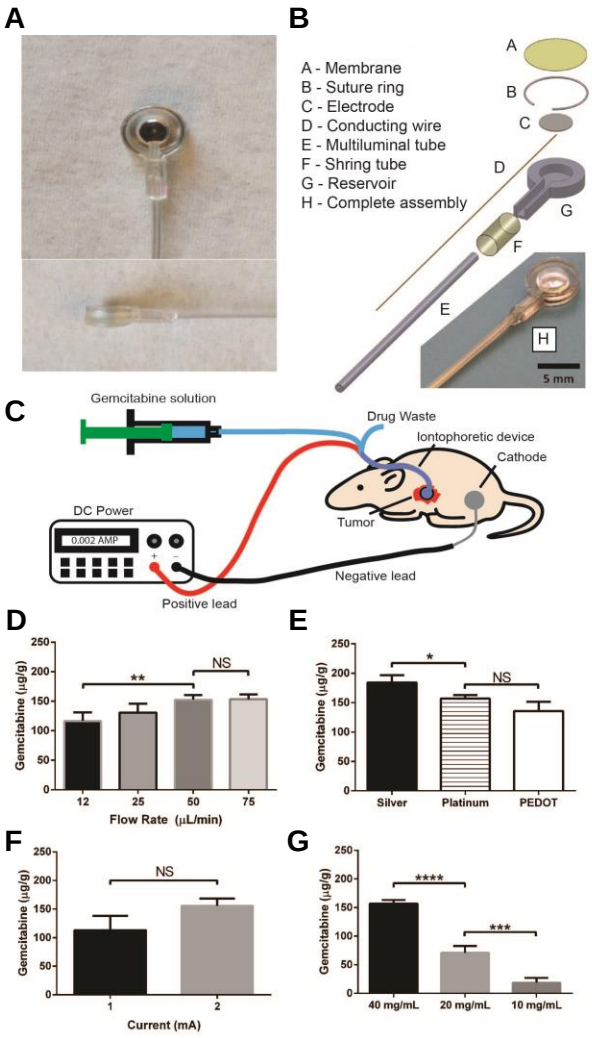

Figure 2.1. Iontophoretic devices used for the delivery of gemcitabine to solid tumors. (A) Front and side images of an implantable device and (B) the corresponding assembly. Animal treatment setups in the (C) pancreatic cancer models where the drug is supplied to the device using a syringe pump and electrical current via a DC power supply. Positive and negative leads connect to the device (anode) and counter electrode (cathode). Device parameters including (D) drug influx rate, (E) electrode material, (F) applied current, and (G) drug concentration were evaluated for drug delivered in tissue surrogates (2 wt% agarose). * $P < 0.05$, ** $P < 0.01$, *** $P < 0.001$, and **** $P < 0.0001$.

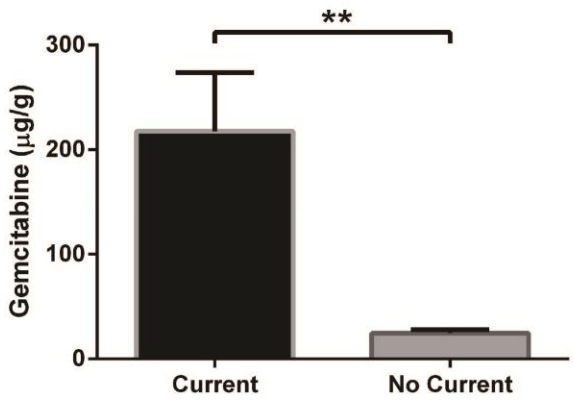

Figure 2.2. Role of current on drug transport in ex vivo human tissue. Gemcitabine transport through PDX tumor tissue as a function of current – 2 mA of current was applied for 10 minutes compared to passive diffusion control (n = 6 per treatment group). **P < 0.01.

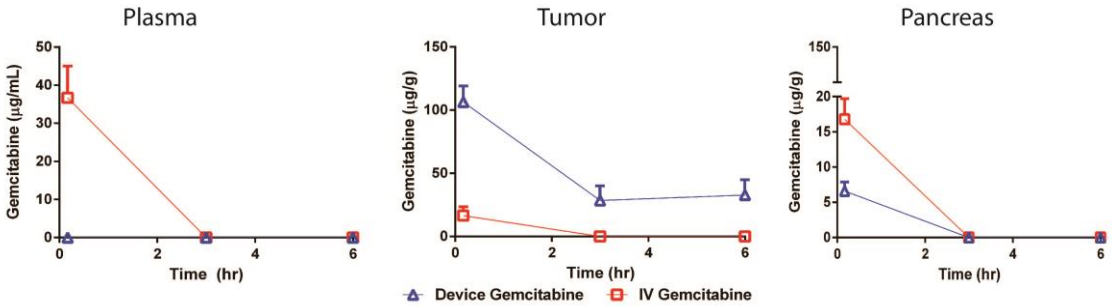

Figure 2.3. PK of gemcitabine delivered by iontophoretic devices into an orthotopic PDX model of pancreatic cancer. Mice (n = 3 - 5 per group) were administered a single treatment of gemcitabine through the device. Organs were collected from each animal at various times, and total gemcitabine concentrations were analyzed (mean ± SEM). Limit of gemcitabine quantitation was 1 μg/mL.

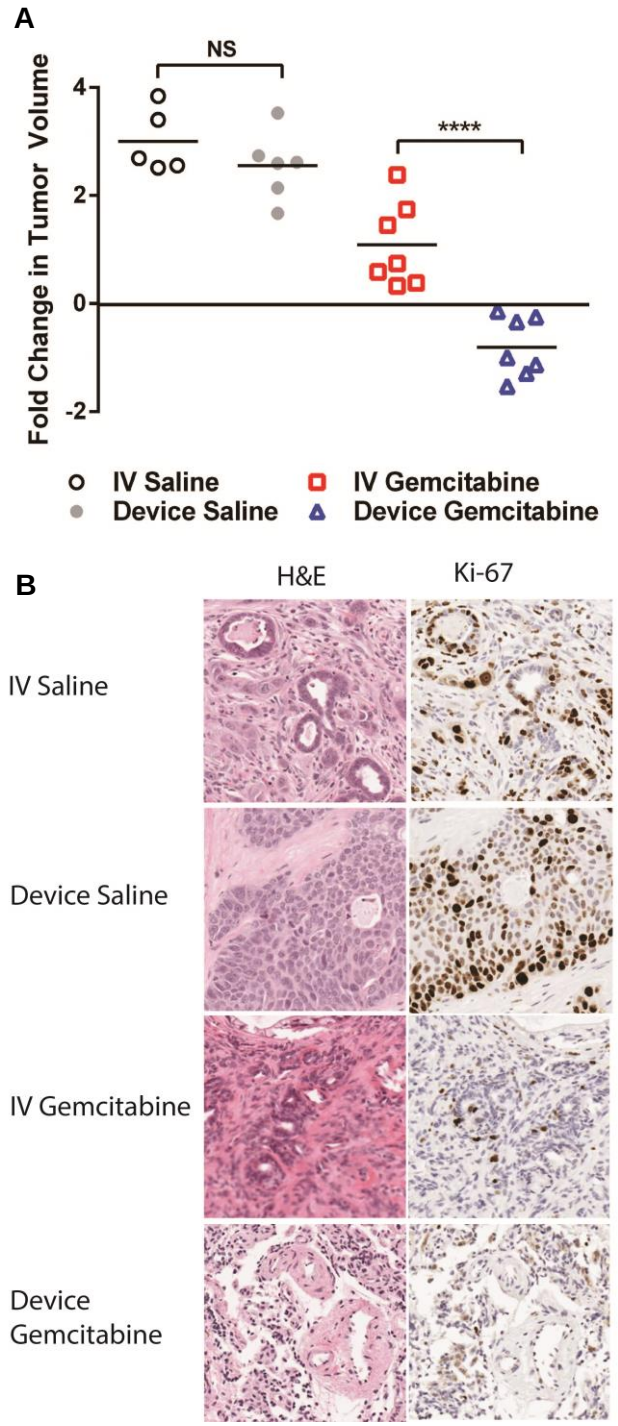

Figure 2.4. Therapeutic effect of gemcitabine delivered iontophoretically in a pancreatic cancer PDX model. (A) Efficacy of device gemcitabine, IV gemcitabine, device saline and IV saline in PDX mice treated twice a week for 7 weeks. Data are fold change in tumor volume (log2) (n = 7 for IV and device gemcitabine, n = 5-6 for IV and device saline). (B) Histological staining of the tumors for Ki-67 at 10X. NS – not significant, **** $P < 0.0001$.

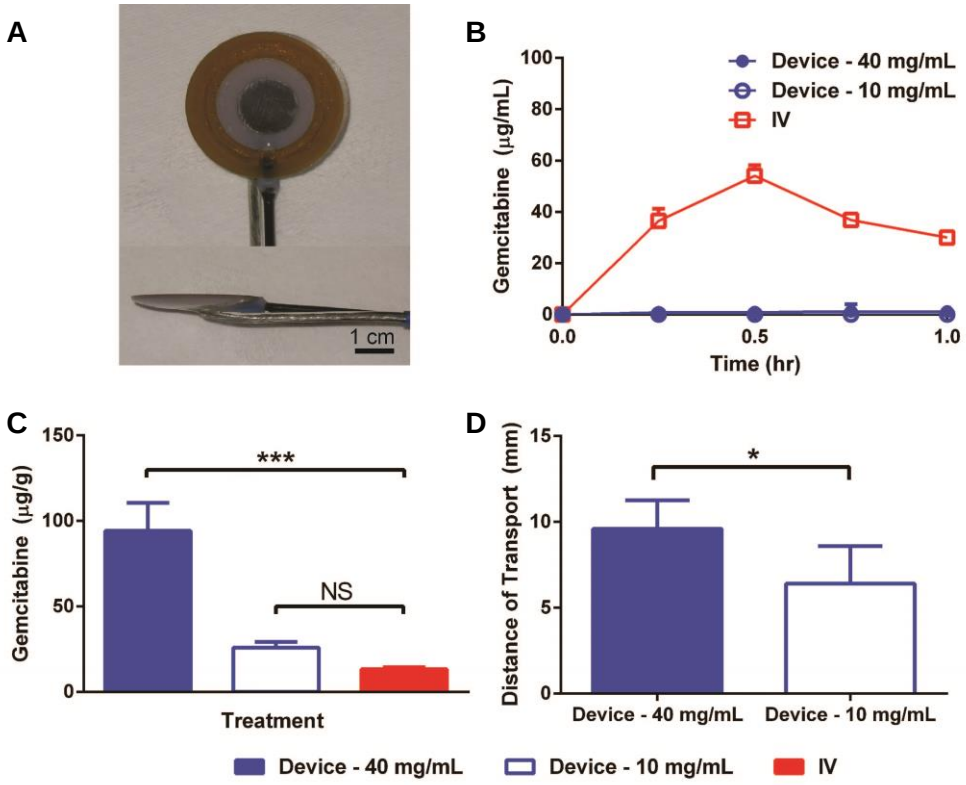

Figure 2.5. Evaluation of single device treatments in a large animal model. (A) Canine device to be implanted directly onto the pancreas. (B) Plasma PK of gemcitabine during the single device treatment. Organs were removed 1 hour after the initiation of treatment and gemcitabine content was quantified. (C) Amount of gemcitabine in the pancreas of dogs after the administration of a single device treatment using 40 mg/mL or 10 mg/mL gemcitabine or IV gemcitabine (1 g/m2). (D) Distance of gemcitabine transport away from the device and into the pancreatic tissue. Data are means ± SEM, NS – not significant, * $P < 0.05$, *** $P < 0.001$.

CHAPTER 3: LOCAL IONTOPHORETIC ADMINISTRATION OF CISPLATIN FOR THE TREATMENT OF BREAST CANCER

3.1 Overview

Parenteral and oral routes have been the traditional methods of administering cytotoxic agents to cancer patients. Unfortunately, the maximum potential effect of these cytotoxic agents has been limited due to systemic toxicity and poor tumor perfusion. In an attempt to improve the efficacy of cytotoxic agents while mitigating their side effects, we have developed modalities for the localized iontophoretic delivery of cytotoxic agents. These pressurized, reservoir-based iontophoretic devices were designed to be implanted proximal to the tumor with external control of power and drug flow. Two distinct orthotopic mouse models of cancer were evaluated for device efficacy and toxicity. In the mouse models, device delivery of cytotoxic agents resulted in enhanced drug accumulation in the tumor and tumor shrinkage. These devices have potential paradigm shifting implications for the treatment of breast, pancreatic, and other solid tumors.

3.2 Introduction

Chemotherapy has had an immeasurable impact on the field of oncology with its inception in the 1940s [1]. Cytotoxic and molecularly-targeted agents have become the mainstay of cancer therapy [2]. However, the maximum potential effect of these therapies

has not been achieved due to secondary toxicities associated with systemic delivery. Many systemically administered chemotherapies place patients at high risk for infection, organ damage, and disability [3]. Furthermore, certain types of solid tumors, such as pancreatic, are perfusion limited [4]. Dense stromal environments and poor vascularization impede diffusion, reducing drug exposure to the primary tumor [5-7]. This impaired drug delivery has contributed to the dreadful prognosis and lack of significant clinical advancements in treatment of certain solid tumors [4,6-7]. To improve the efficacy of chemotherapies and mitigate their side effects, new drug delivery strategies are necessary to concentrate the drug in the tumor site while sparing off-target tissue toxicities.

Local drug delivery technologies offer a promising alternative to systemic delivery. They exist in a variety of form factors designed to facilitate the delivery of drug directly to the site of disease in a controlled manner. Many of these are biodegradable polymeric depots designed to maintain therapeutic concentrations of drug at the tumor site for a prolonged period of time. However, only a small subset of these technologies has demonstrated potentially curative preclinical results for cancer applications, and far fewer have progressed toward clinical practice. A key challenge of many of these local drug delivery systems, particularly polymeric-drug eluting technologies like the Gliadel wafer, has been diffusion limitations [8]. The lack of spatial distribution of drugs and elevated interstitial fluid pressures in solid tumors have relegated the use of many local drug delivery systems to post-surgical therapy [9]. A subset of local drug delivery devices involves the use of electric fields to drive drugs into the area of greatest need in a technique known as iontophoresis. Iontophoretic devices are capable of overcoming diffusion barriers by electrorepulsive and electroosmotic forces [10-12]. Advances in urologic and ophthalmologic devices have

enabled the effective iontophoretic delivery of mitomycin C and dexamethasone to tissues while reducing the systemic effects of these drugs [13-16]. Here, we developed and investigated a new iontophoretic device platform for the local delivery of cytotoxic therapies to solid tumors. These pressurized, reservoir-based iontophoretic devices were designed to be implanted proximal to the tumor with external user control of power and drug flow.

To evaluate the broad application of these iontophoretic devices as potential anti-cancer therapies, we elected to test the devices in a diverse set of orthotopic breast cancer models [17-20]. We describe an in-depth preclinical characterization of iontophoretic delivery of cytotoxic agents. We report that these devices deliver high levels of cytotoxic drugs, reduce systemic exposure of the drugs, and potently impact tumor growth. These devices offer an entirely new modality for the treatment of cancer.

3.3 Results

3.3.1 Device Development

Our devices were designed to adapt conventional iontophoretic drug delivery techniques. Figure 3.1A-C showcases the device, the assembly, and the setup for animal treatments. The devices were composed of a polydimethylsiloxane reservoir, a silver electrode, and an inlet and outlet for continuous drug flow through the reservoir. This continuous drug flow maintained a constant drug concentration around the electrode and pressure within the device. Under an applied electric potential, the drug was transported in the direction normal to the electrode and into the tissue.

3.3.2 Drug Transport in Human Tissue

The transport of cisplatin into ~1 mm thick ex vivo human skin was evaluated using a modified Franz diffusion cell with the device directly above the skin instead of a donor chamber. One or 0 mA of current was applied for 25 minutes, and the skin and solution were snap frozen, processed, and analyzed by inductively coupled plasma-mass spectrometry (ICP-MS). The application of current resulted in an 11.4-fold increase in platinum transported into the human skin compared to passive diffusion (Figure 3.2). In the receptor compartment, we found 24.8 ± 18.8 ng/mL platinum when current was applied but no detectable amount of platinum for the passive diffusion control. Murine skin was evaluated using the same method revealing similar drug transport into the skin but larger transport through the skin.

3.3.3 Pharmacokinetics and Biodistribution of Cisplatin

Figure 3.3 shows a typical study in which the device delivery of cisplatin was evaluated in an orthotopic SUM149 xenograft model of breast cancer. The concurrent device and IV delivery of cisplatin was added as an arm of the study based upon the low systemic exposure of cisplatin after device treatments. A single treatment was administered after adhesion of the device to the skin above the tumor. Platinum plasma exposure as measured by AUC of the concentration vs time curve for device delivery, IV, and device + IV delivery were 2.0, 9.9, and 10.7 hr*µg/mL, respectively. In addition, tumor AUC for device, IV (5 mg/kg), and device + IV (5 mg/kg) delivery were 30.2, 42.4, and 83.4 hr*µg/g, respectively. Furthermore, there were significant differences in cisplatin accumulation in the left inguinal

mammary, kidney, skin, inguinal lymph node, and right inguinal mammary for the two different routes of cisplatin administration.

3.3.4 Device Efficacy

This platform technology was further evaluated in orthotopic breast cancer models – SUM149 xenograft and T11 syngeneic models (Figure 3.4). In both models, we compared the efficacy of device cisplatin, IV cisplatin, device + IV cisplatin, device saline, and IV saline (Figure 3.4A-B and D-E). Once the SUM149 xenograft tumors reached ~50 mm^3, the mice were treated with device cisplatin, IV cisplatin (5 mg/kg), device + IV cisplatin (5 mg/kg), device saline, or IV saline every week for a total of four doses. Mice bearing T11 tumors received two doses of the same test arms 1 week apart beginning 5 days after inoculation (~20 mm^3). The number of treatments varied across different tumor models owing to differences in tolerability of treatments. Device cisplatin and IV cisplatin both resulted in significant tumor growth inhibition compared to the controls in the SUM149 ($p = 0.0002$) and T11 models ($p < 0.0001$) (Figure 3.4A and E). Device + IV cisplatin resulted in significant tumor growth inhibition, outperforming device cisplatin and IV cisplatin in both tumor models ($p = 0.0002$). We also assessed the effects of device treatment on overall survival in the tumor models. Device cisplatin, IV cisplatin, and device + IV cisplatin extended the lifespan from a median of 49 days to 60, 68, and past 100 days, respectively, in the SUM149 model ($p < 0.0001$) (Figure 3.4B). Device cisplatin, IV cisplatin, and device + IV cisplatin extended the lifespan from a median of 10 days to 20, 22, and 32 days, respectively, in the T11 model ($p < 0.0001$) (Figure 3.4D). The skin of the mice after four

weekly device treatments showed no scarring or deformation (Figure 3.4C). Device cisplatin was better tolerated based on histological staining of the kidneys for a sensitive molecular marker of DNA damage and repair, γH2AX, compared to IV cisplatin and device + IV cisplatin (Figure 3.5). In addition, histological samples from tumors post treatment revealed almost equivalent γH2AX staining from device cisplatin and IV cisplatin-treated mice and greater γH2AX staining in device + IV cisplatin-treated mice (Figure 3.4F).

We next determined whether the addition of radiotherapy to the device delivery of cisplatin, a well-known radiosensitizing agent, could improve the therapeutic effect of the treatment. Mice bearing orthotopic T11 tumors received a single dose of the radiation (10 Gy), device cisplatin, device cisplatin + radiation (10 Gy), IV cisplatin (5 mg/kg), IV cisplatin + radiation (10 Gy), device + IV cisplatin (5 mg/kg), or device cisplatin + IV cisplatin (5 mg/kg) + radiation (10 Gy) 5 days after inoculation (~20 mm^3). There were three major cohorts of response (Figure 3.4G and H). Mice treated with a single dose of radiation, device cisplatin, or IV cisplatin resulted in similar tumor growth rates and survival; compared to the no treatment control, a single dose of radiation, device cisplatin, or IV cisplatin resulted in significant tumor growth inhibition ($p < 0.0001$) and survival ($p < 0.0001$). Mice treated with a single dose of device cisplatin + radiation, IV cisplatin + radiation, or device + IV cisplatin also resulted in similar tumor growth rates and survival; compared to the radiation, device cisplatin, and IV cisplatin treatments, a single dose of device cisplatin + radiation, IV cisplatin + radiation, or device + IV cisplatin resulted in significantly greater tumor growth inhibition ($p < 0.0001$) and survival ($p < 0.0001$), indicating that the addition of radiotherapy to the device and IV treatments improved tumor growth inhibition. Device + IV cisplatin + radiation outperformed all other treatment groups in tumor growth inhibition

and survival; compared to the device cisplatin + radiation, IV cisplatin + radiation, and device + IV cisplatin treatments, a single dose of device + IV cisplatin + radiation resulted in non-statistically significant tumor growth inhibition ($p = 0.084$) but significantly greater survival ($p < 0.0002$). Overall, the addition of radiation to device cisplatin, IV cisplatin, and device + IV cisplatin significantly improved survival ($p < 0.0001$).

3.4 Discussion

It is believed that local delivery of chemotherapies will have a revolutionary impact on the treatment of cancer by maximizing the effect at the target site and sparing off-target tissue toxicities [9]. Despite this belief, the translation of the local drug delivery technologies from basic research into everyday cancer treatments has remained elusive. We decided to take an iontophoretic approach to address the issue that plagues the success of these technologies – limited drug penetration. Iontophoresis is capable of overcoming considerable flow and pressure gradients, particularly those found in solid tumors [13]. In addition, a large number of small molecule drugs are capable of being delivered by iontophoresis [15, 21-23].

Here, we show that iontophoretic devices can deliver substantial amounts of drugs to the site of interest with limited systemic exposure. Our preclinical results suggest that device delivery of cisplatin may potentiate the current treatment of solid tumors by enhancing the therapeutic index of the drugs. In addition, the co-administration of systemic therapy, device therapy, and radiotherapy proved feasible and significantly improved tumor growth inhibition and survival in breast cancer models.

Although our iontophoretic devices enable significant local drug transport, their efficacy could be further improved by potentially altering the dosing schedule, optimizing drug formulations, and configuring the device according to tumor shape and surrounding anatomy. Because of the high drug concentrations in the tumor and low level of systemic exposure after a single treatment, the number of device treatments could be increased. Drug formulation plays an important role in the iontophoretic delivery of drugs through competing ions and electroosmotic flow, and the evaluation of formulation excipients could improve total drug delivered and distance of drug transport [24]. Configuring these devices to fit the shape of the tumor and surrounding anatomy would improve efficacy by creating better contact between the device and tumor tissue and, in the case of pancreatic cancer, strategically delivering the cytotoxic agents to the area that would enable tumor resection. Furthermore, some key parameters that need to be understood for success in the clinic are the adequacy of drug penetration for humans and the scaling of the treatment to address larger human tumors.

3.5 Materials and Methods

3.5.1 Device Fabrication

Iterative device design was performed using a 3D computer-aided design software (SolidWorks). An 8.6 mm silver disc was soldered to a 36-gauge copper wire and embedded in a polydimethylsiloxane (Sylgard 184) reservoir prior to crosslinking. The copper wire was thread through one multi-luminal tube, and the tube was inserted into the reservoir for influx

of drug. Another multi-luminal tube was inserted on the contralateral side of the reservoir for drug efflux.

3.5.2 Ex Vivo Studies

De-identified human skin was provided by the cooperative human tissue network. The frozen skin was thawed and sectioned into 2 x 2 cm squares prior to drug transport studies. The transport of cisplatin in skin was evaluated using a modified Franz diffusion cell with the device directly above the skin. The receptor chamber was filled with 5mL of normal saline. One or 0 mA of current was applied for 25 minutes, and the skin and solution were snap frozen, processed by nitric acid, and analyzed by ICP-MS.

3.5.3 Animal Studies

All procedures were approved by the appropriate Institutional Animal Care and Use Committee before initiation. All animals used in PK, biodistribution, and efficacy studies were allowed to acclimate for at least 1 week in the animal facilities before experimentation. Animals were exposed to a 12-hour light/dark cycle and received food and water ad libitum through the studies. For quantitation of cisplatin plasma concentrations, blood samples were collected into lithium heparin tubes and plasma was generated and frozen with liquid nitrogen; tissue and device were extracted and snap frozen with liquid nitrogen and stored at -80 °C. Total platinum was extracted from frozen plasma and organs using a nitric acid degradation method and analyzed by ICP-MS [25].

3.5.4 PK Studies

Five million SUM149 cells resuspended in Matrigel (50:50) were injected into the left inguinal mammary fat pad of 4-8 week old athymic nude mice. Devices were transdermal adhered onto the skin (3M Vetbond) above the orthotopic tumors when they reached a single dimension of 5-7 mm. The cisplatin solutions used for device delivery were formulated at pH 5.9 (APP Pharmaceuticals, LLC), and the cisplatin used for IV delivery was administered directly from the clinical formulation. A constant DC power supply was used to provide power to the device. The positive lead was connected to the device wire, and the negative lead was connected to a silver chloride electrode placed on the mouse's skin with electrolyte gel. A syringe pump was used to circulate the cisplatin solution through the device at a flow rate of 50 µL/min over a period of 10 minutes. When the device was powered, drug was driven from the device reservoir, through the membrane and into the tumor tissue following the path of the electrical current. Upon completion of the treatment, the device was emptied of drug solution. Terminal bleeds were performed. The mice were treated with a single transdermal iontophoretic dose of cisplatin or 5 mg/kg bolus of cisplatin via tail vein. Plasma, tumor, skin, kidney, left and right inguinal mammary glands, and inguinal lymph node were collected at 0.5, 1, 6, and 24 hours after administration.

3.5.5 Efficacy Studies

The technical protocol for device treatments was identical to the PK studies. Mice were treated two or four times weekly using device cisplatin, IV cisplatin (5 mg/kg), device + IV (5 mg/kg) cisplatin, device saline (0.9% NaCl), or IV saline. Tumors derived from

BALB/cTP53$^{-/-}$ orthotopic mammary gland transplant line (T11) were passage in BALB/c wild-type mice by subcutaneous injection of five hundred thousand cells resuspended in matrigel (50:50) into the left inguinal mammary gland. The day before scheduled treatment, the mice were shorn with clippers, and the residual hair was removed using Nair. For the radiation studies, at two hours post injection, the tumors were subjected to a dose of 10 Gy with XRAD 320. Mice were shielded with a specially designed lead cover allowing irradiation of the tumor site and minimal radiation to other organs.

3.5.6 PK and Statistical Analyses

PK parameters were assessed with Phoenix WinNonLin (version 6.0). Analysis of variance methods (ANOVA), using generalized linear models, were used to make comparisons of continuous values between groups. Pairwise comparisons were made when an overall difference was detected. For figure 5A, D, and G, comparisons were made between groups at two time points: 1) when all mice were still alive (day 28, 9, 9) and 2) when all mice on treatment were still alive (day 42, 16, 15). AUC was used as the summary measure for figure 6B, and comparisons were made use ANOVA as well. For survival data, the Kaplan Meier method and Log-rank tests were used to make comparisons between groups. Unadjusted p-values are reported for pairwise comparisons, when an overall difference was detected. All analyses were done using SAS v9.3 (Cary, NC).

3.6 Additional Support

We would like to thank Charlene Santos, the UNC animal studies core, and tissue procurement facility for their contributions to this work. This work was supported by funding from the University Cancer Research Fund, and an NIH Pioneer Award.

3.7 REFERENCES

[1] L.S. Goodman, M.M. Wintrobe, W. Dameshek, M.J. Goodman, M.A. Gilman, M.T. McLennan. Use of Methyl-Bis(Beta-Chloroethyl)amine Hydrochloride and Tris(Beta-Chloroethyl)amine Hydrochloride for Hodgkin's Disease, Lymphosarcoma, Leukemia and Certain Allied and Miscellaneous Disorders. J. Am. Med. Assoc. 132, 126-132 (1946).

[2] A. Jemal, R. Siegel, E. Ward, Y. Hao, J. Xu, T. Murray, M.J. Thun. Cancer Statistics, 2008. C.A. Cancer. J. Clin. 58, 71-96 (2008).

[3] D. Schiff D, P.Y. Wen, M.J. van den Bent. Neurological adverse effects caused by cytotoxic and targeted therapies. Nat. Rev. Clin. Onc. 6, 596-603 (2009).

[4] K.P. Olive, M.A. Jacobetz, C.J. Davidson, A. Gopinathan, D. McIntyre, D. Honess, B. Madhu, M.A. Goldgraben, M.E. Caldwell, D. Allard, K.K. Frese, G. Denicola, C. Feig, C. Combs, S.P. Winter, H. Ireland-Zecchini, S. Reichelt, W.J. Howat, A. Chang, M. Dhara, L. Wang, F. Rückert, R. Grützmann, C. Pilarsky, K. Izeradjene, S.R. Hingorani, P. Huang, S.E. Davies, W. Plunkett, M. Egorin, R.H. Hruban, N. Whitebread, K. McGovern, J. Adams, C. Iacobuzio-Donahue, J. Griffiths, D.A. Tuveson. Inhibition of Hedgehog Signaling Enhances Delivery of Chemotherapy in a Mouse Model of Pancreatic Cancer. Science 324, 1457-1461 (2009).

[5] A.I. Minchinton, I.F. Tannock, Drug Penetration in Solid Tumors. Nat. Rev. Cancer 6, 583-592 (2006).

[6] I.F. Tannock, C.M. Lee, J.K. Tunggal, D.S. Cowan, M.J. Egorin. Limited penetration of anticancer drugs through tumor tissue: a potential cause of resistance of solid tumors to chemotherapy. Clin. Cancer Res. 8, 878 (2002).

[7] J.K. Tunggal, D.S.M. Cowan, H. Shaikh, I.F. Tannock. Penetration of anticancer drugs through solid tissue: a factor that limits the effectiveness of chemotherapy for solid tumors. Clin. Cancer Res. 5, 1583-1586 (1999).

[8] L.K. Fung, M.G. Ewend, A. Sills, E.P. Sipos, R. Thompson, M. Watts, O.M. Colvin, H. Brem, W.M. Saltzman. Pharmacokinetics of interstitial delivery of carmustine, 4-hydroperoxycyclophosphamide, and paclitaxel from a biodegradable polymer implant in the monkey brain. Cancer Res. 58, 672-684 (1998).

[9] J.B. Wolinsky, Y.L. Colson, M.W. Grinstaff. Local drug delivery strategies for cancer treatment: Gels, nanoparticles, polymeric films, rods, and wafer. J. Control. Rel. 159, 14-26 (2012).

[10] M.R. Prausnitz, S. Mitragotri, R. Langer. Current status and future potential of transdermal drug delivery. Nat. Rev. Drug Disc. 3, 115-124 (2004).

[11] Y.N. Kalia, A. Naik, J. Garrison, R.H. Guy. Iontophoretic drug delivery. Adv. Drug Deliv. Rev. 59, 619-658 (2004).

[12] V. Merino, A. Lopez, Y.N. Kalia, R.H. Guy. Electrorepulsion versus electroosmosis: effect of pH on the iontophoretic flux of 5-fluorouracil. Pharm. Res. 16, 758-761 (1999).

[13] S.M. Di Stasi, A. Giannantoni, R. Massoud, S. Dolci, P. Navarra, G. Vespasiani, R.L. Stephen. Electromotive versus passive diffusion of mitomycin C into human bladder wall: concentration-depth profile studies. Cancer Res. 59, 4912-4918 (1999).

[14] S.M. Di Stasi, A. Giannantoni, A. Giurioli, M. Valenti, G. Zampa, L. Storti, F. Attisani, A. De Carolis, G. Capelli, G. Vespasiani, R.L. Stephen. Sequential BCG and electromotive mitomycin versus BCG alone for high-risk superficial bladder cancer: a randomised controlled trial. Lancet Onc. 7, 43-51 (2006).

[15] S.M. Di Stasi, M. Valenti, C. Verri, E. Liberati, A. Giurioli, G. Leprini, F. Masedu, A.R. Ricci, F. Micali, G. Vespasiani. Electromotive instillation of mitomycin immediately before transurethral resection for patients with primary urothelial non-muscle invasive bladder cancer: a randomised controlled trial. Lancet Onc. 12, 871-879 (2011).

[16] A.E. Cohen, C. Assang, M.A. Patane, S. From, M. Korenfeld. Evaluation of Dexamethasone Phosphate Delivered by Ocular Iontophoresis for Treating Noninfectious Anterior Uveitis. Ophthal. 119, 66-73 (2012).

[17] R.J. Torphy, C.J. Tignanelli, J.W. Kamande, R.A. Moffitt, S.G. Herrera Loeza, S.A. Soper, J.J. Yeh. Circulating tumor cells as a biomarker of response to treatment in patient-derived xenograft mouse models of pancreatic adenocarcinoma. PLoS One 9 (2014).

[18] N.F. Neel, J.K. Stratford, V. Shinde, J.A. Ecsedy, T.D. Martin, C.J. Der, J.J. Yeh. Response to MLN8237 in pancreatic cancer is not dependent on RalA phosphorylation. Mol. Cancer Ther. 13, 122-33 (2013).

[19] J. Usary, W. Zhao, D. Darr, P.J. Roberts, M. Liu, L. Balletta, O. Karginova, J. Jordan, A. Combest, A. Bridges, A. Prat, M.C.U. Cheang, J.I. Herschkowitz, J.M. Rosen, W. Zamboni, N.E. Sharpless, C.M. Perou. Predicting Drug Responsiveness in Human Cancers Using Genetically Engineered Mice. Clin. Cancer Res. 19, 4889-489 (2013).

[20] D. Zhang, T.A. LaFortune, S. Krishnamurthy, F.J. Esteva, M. Cristofanilli, P. Liu, A. Lucci, B. Singh, M.C. Hung, G.N. Hortobagyi, N.T. Ueno. Epidermal growth factor receptor tyrosine kinase inhibitor reverses mesenchymal to epithelial phenotype and inhibits metastasis in inflammatory breast cancer. Clin. Cancer Res. 15, 6639-6648 (2009).

[21] M. Morfouace, A. Shelat, M. Jacus, B.B. Freeman, D. Turner, S. Robinson, F. Zindy, Y.D. Wang, D. Finkelstein, O. Ayrault, L. Bihannic, S. Puget, X.N. Li, J.M. Olson, G.W. Robinson, R.K. Guy, C.F. Stewart, A. Gajjar, M.F. Roussel. Pemetrexed and gemcitabine as combination therapy for the treatment of group3 medulloblastoma. Cancer Cell 25, 516-529 (2014).

[22] M. Komuro, K. Suzuki, M. Kanebako, T. Kawahara, T. Otoi, K. Kitazato, T. Inagi, K. Makino, M. Toi, H. Terada. Novel iontophoretic administration method for local therapy of breast cancer. J. Con. Rel. 168, 298-306 (2013).

[23] S. Gungor, M.B. Delgado-Charro, V. Masini-Eteve, R.O. Potts, R.H. Guy. Transdermal flux predictions for selected selective estrogen receptor modulators (SERMs): comparison with experimental results. J. Con. Rel. 172, 601-606 (2010).

[24] R.H. Guy, Y.N. Kalia, M.B. Delgado-Charro, V. Merino, A. Lopez, D. Marro. Iontophoresis: electrorepulsion and electroosmosis. J. Con. Rel. 64, 129-132 (2000).

[25] W.P. Caron, J.C. Lay, A.M. Fong, N.M. La-Beck, P. Kumar, S.E. Newman, H. Zhou, J.H. Monaco, D.L. Clarke-Pearson, W.R. Brewster, L. Van Le, V.L. Bae-Jump, P.A. Gehrig, W.C. Zamboni. Translational studies of phenotypic probes for the mononuclear phagocyte system and liposomal pharmacology. J. Pharmacol. Exp. Ther. 347, 599-606 (2013).

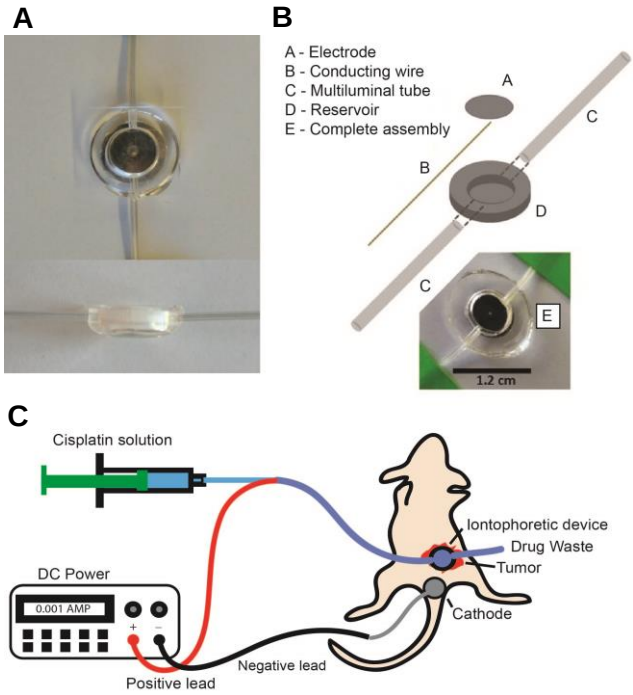

Figure 3.1. Iontophoretic devices used for the delivery of cisplatin to solid tumors. (A) front and side images of a transdermal device, and (B) the corresponding assemblies. Animal treatment setups in the (C) breast cancer models where the drug is supplied to the device using a syringe pump and electrical current via a DC power supply. Positive and negative leads connect to the device (anode) and counter electrode (cathode).

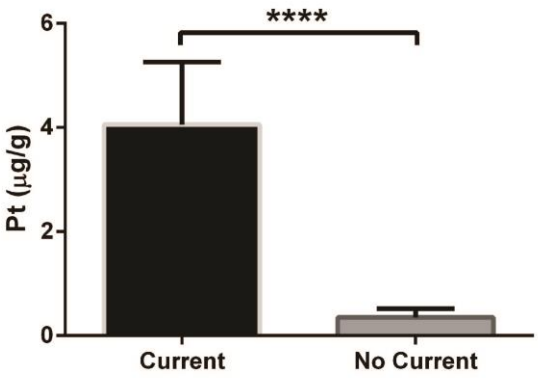

Figure 3.2. Role of current on drug transport in ex vivo human tissue. Cisplatin transport through human skin as a function of current – 1 mA of current was applied for 25 minutes compared to passive diffusion control (n = 5 per treatment group). **** $P < 0.0001$.

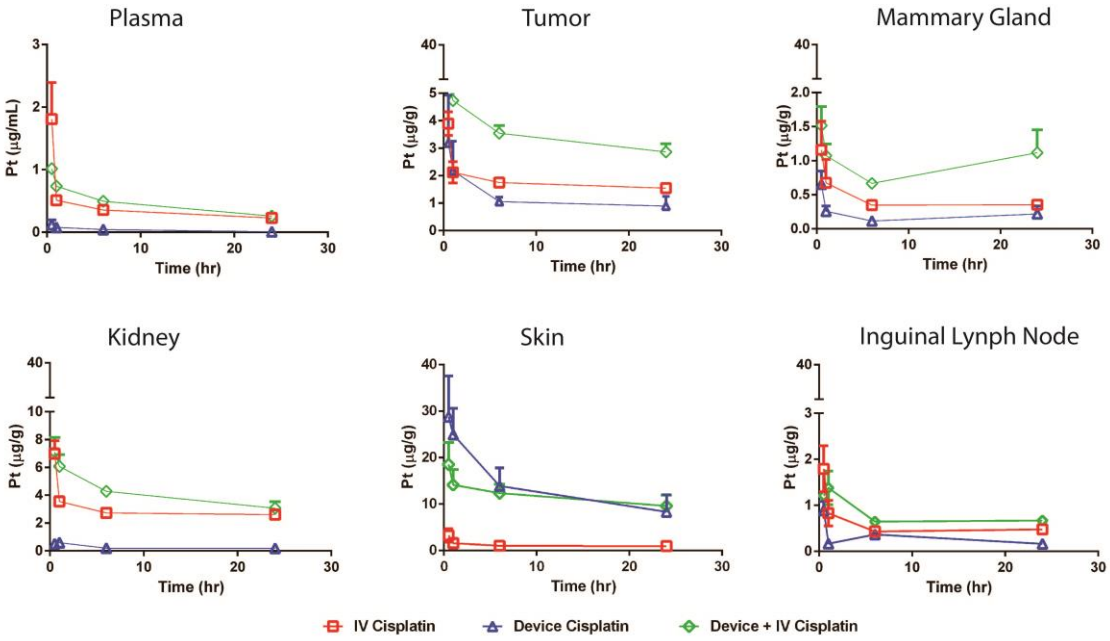

Figure 3.3. PK of cisplatin delivered by iontophoretic devices into SUM149 orthotopic xenografts of breast cancer. Mice (n = 5 per group) were administered a single treatment of cisplatin through the device. Organs were collected from each animal at various times, and total platinum concentrations were analyzed (mean ± SEM). Limit of platinum quantitation was 5 ng/mL.

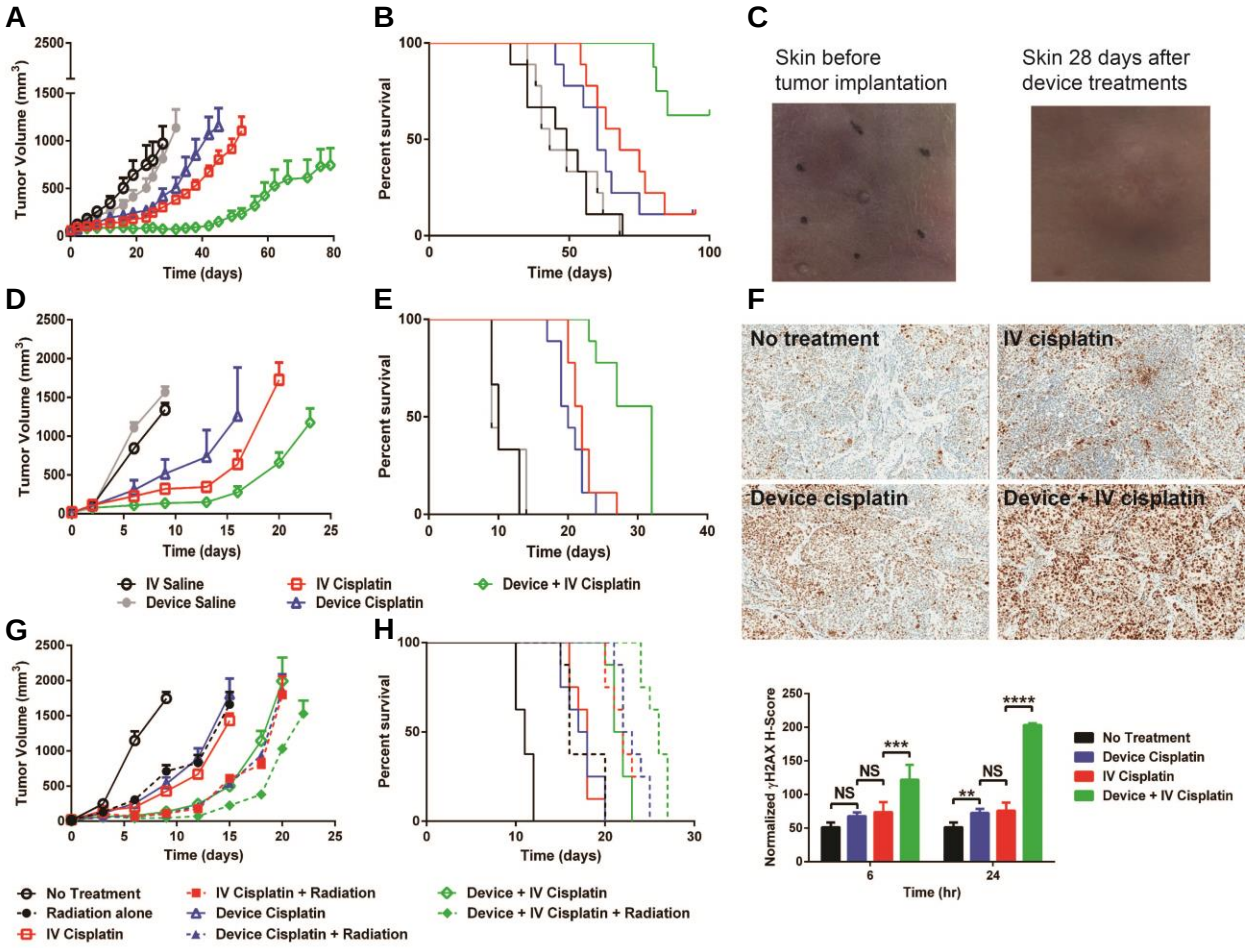

Figure 3.4. Therapeutic effect of cisplatin delivered iontophoretically in mouse tumor xenograft and syngeneic models of breast cancer. (A) Efficacy and (B) survival of device cisplatin, IV cisplatin, device + IV cisplatin, device saline and IV saline in the SUM149 tumor xenograft model treated once a week for a total of four doses (n = 8 – 9 per treatment group). (C) Representative images of murine skin before and after four weeks of device treatment. (D) Efficacy and (E) survival of device cisplatin, IV cisplatin, device + IV cisplatin, device saline and IV saline in the T11 syngeneic model treated once a week for a total of two doses (n = 9 per treatment group). (F) Histological staining of tumors for γH2AX (4X) harvested from SUM149 tumor xenografts 24 hours after a single treatment and quantification of γH2AX staining according to H-score. Next, we evaluated the combinatorial effect of radiation and IV cisplatin, device cisplatin, or IV + device cisplatin in the T11 syngeneic model. (G) Efficacy and (H) survival after a single treatment of no treatment control, radiation, device cisplatin, device cisplatin + radiation, IV cisplatin, IV cisplatin + radiation, device + IV cisplatin, or device + IV cisplatin + radiation (n = 8 per treatment group). Data are mean tumor volumes ± SEM. NS – not significant, ** $P < 0.01$, *** $P < 0.001$, and **** $P < 0.0001$.

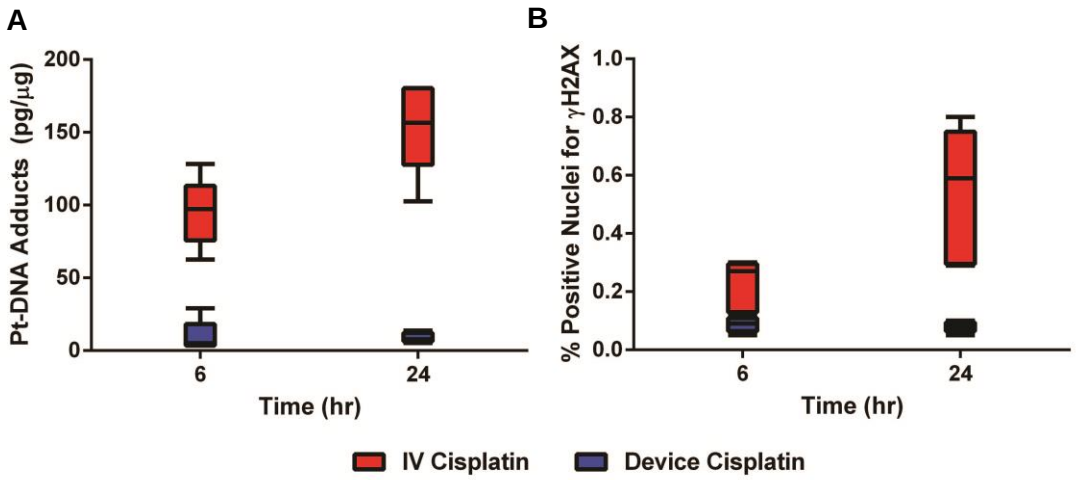

Figure 3.5. Pharmacological evaluation of the short-term renal toxicity after a single device cisplatin treatment. (A) Platinum-DNA adducts and (B) γH2AX staining within the kidney in a SUM149 breast cancer xenograft model (n = 5 per group). Organs were collected from each animal at 6 and 24 hours.

CHAPTER 4: CONCLUSIONS AND FUTURE DIRECTIONS

Here, we show that iontophoretic devices can deliver substantial amounts of drugs to the site of interest with limited systemic exposure. Our preclinical results suggest that device delivery of gemcitabine and cisplatin may potentiate the current treatment of solid tumors by enhancing the therapeutic index of the drugs. In addition, the co-administration of systemic therapy, device therapy, and radiotherapy proved feasible and significantly improved tumor growth inhibition and survival in breast cancer models.

For future studies, the implantable devices should be redesigned to address key issues of gas formation on the electrode, protein buildup on the reservoir membrane, device anchoring onto tumors, and time requirements for device fabrication. The electrochemistry of Pt electrodes produces significant gas pockets that limit the transport of drug and increase the voltage necessary to maintain a constant current. Disruption of the bubbles through physical measures would facilitate greater drug transport and reduce the potential for animals or patients to experience electrical shocks during the treatment. Separation of the inlet and outlet could also improve removal of the bubbles and filling of the drug reservoir. Secondly, the reservoir membrane used within these studies was a 12 kDa cellulose membrane, and for future work, a polytetrafluoroethylene membrane with the same molecular weight cutoff should be considered to reduce protein buildup on the membrane. Furthermore, flaps could be incorporated into the device to allow for suturing the device onto the solid tumor, in order to keep the sutures away from the central device reservoir. Device size and shape could play

a significant role in the effectiveness of drug delivery. Three-dimensional (3D) printing of the device according to computed tomographic imaging of the tumor could be helpful in fitting the device to the patient's anatomy [1]. Important considerations for the 3D printing of the device include the ability to incorporate the metallic electrode within the device and adhesion of the membrane on the device. Post-fabrication processing steps would be necessary to thread the electrode through an opening of the printed device, seal the device using a physical or chemical process, and adhere the membrane on the device reservoir. Addressing these key issues would potentially improve drug transport from a reservoir-based iontophoretic device.

A thorough safety evaluation will be necessary in progressing towards human trials. Evaluation of damage on normal tissue surrounding the implantation and device treatments sites will need to be performed in large animals. For the transdermal delivery of a cytotoxic agent, one would need to follow-up on long-term ramifications of local skin irritation and the possibility of scar formation. Determining systemic exposure as a function of device surface area will be important to understand the device size constraints. Furthermore, delineating drug versus device effects will be necessary in identifying the functionality of the drug-device combination. Safety evaluation of the device in combination with radiation and systemic chemotherapy could also be necessary as the treatment would likely be used in combination with other therapies.

With the ability to locally deliver toxic regimens to solid tumors, it may be possible to evaluate the delivery of abandoned drugs and less water-soluble drugs. Güngör et al. evaluated the delivery of less soluble drugs by using organic/aqueous solutions [2]. Similar to Sethi et al., the use of wortmannin and other such drugs could improve radio-sensitivity of

the drugs while reducing toxicity [3]. Peptide and protein delivery is also feasible and could potentially allow for an immunomodulatory component of the device treatment [4]. Furthermore, alternative device embodiments should be evaluated, such as intravascular and endoscopic approaches (Figure 4.1).

Overall, the challenge of using iontophoresis for the treatment of cancer is identifying the right drug–disease combination for which iontophoresis represents real added-value over and above the existing approach and alternative options. A prime example outside of oncology is the delivery of lidocaine. Iontophoresis is able to induce local anesthesia much faster than a typical, topical cream, but the use of the device is more complex, requiring more health professional time to set up and explain to the patient, and is more expensive. Therefore, will shortening of time required for the pharmacological effect to be induced a sufficient benefit to outweigh the less positive features? In the field of oncology, iontophoretic devices could play an important role as an adjunct therapy. The addition of the iontophoretic device delivery to systemic therapy could build upon the recent success of FOLFIRINOX and gemcitabine + abraxane in the treatment of metastatic pancreatic cancer.

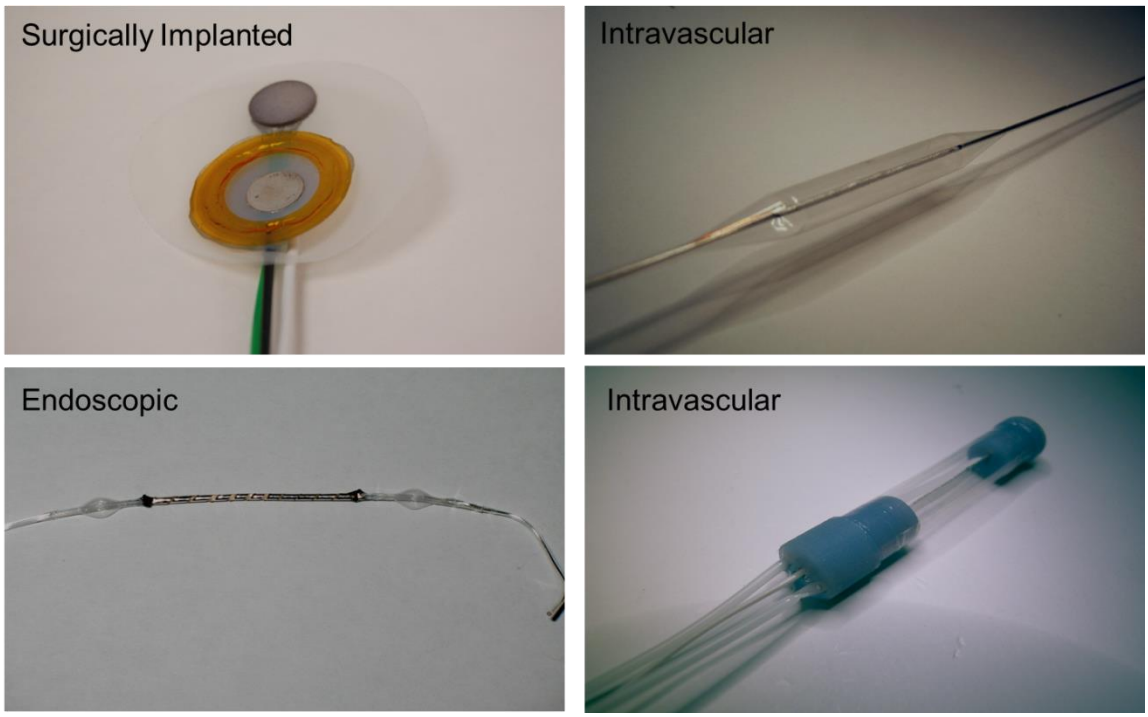

Figure 4.1. Iontophoretic devices for the treatment of internal body cancers.

4.1 REFERENCES

[1] D.A. Zopf, S.J. Hollister, M.E. Nelson, R.G. Ohye, G.E. Green. Bioresorbable Airway Splint Created with a Three-Dimensional Printer. N. Engl. J. Med. 368, 2043-2045 (2013).

[2] S. Güngör, M.B. Delgado-Charro, V. Masini-Etévé, R.O. Potts, R.H. Guy. Transdermal flux predictions for selected selective oestrogen receptor modulators (SERMs): comparison with experimental results. J Control Release. 172, 601-606 (2013).

[3] S. Karve, M.E. Werner, R. Sukumar, N.D. Cummings, J.A. Copp, E.C. Wang, C. Li, M. Sethi, R.C. Chen, ME. Pacold, A.Z. Wang. Revival of the abandoned therapeutic wortmannin by nanoparticle drug delivery. Proc. Natl. Acad. Sci. U. S. A. 109, 8230-8235 (2012).

[4] R.H. Guy. Interview with Richard H Guy by Hannah Coaker. Ther. Deliv. 5, 123-128 (2014).